

**Supporting Information: A Fragment  
Diabatization Linear Vibronic Coupling  
Model For Quantum Dynamics Of  
Multichromophoric Systems: Population Of  
The Charge Transfer State In The  
Photoexcited Guanine Cytosine Pair**

# Contents

<b>S1 Additional Numerical Details</b>	<b>S-3</b>
S1.1 Diabatization Scheme in TD-DFT . . . . .	S-3
S1.2 Absorption Spectra . . . . .	S-6
<b>S2 Electronic Structure Details and Data</b>	<b>S-7</b>
S2.1 Natural Transition Orbitals . . . . .	S-7
S2.2 Adiabatic TD-DFT Minima Calculation Details . . . . .	S-10
S2.3 Normal Modes CAM-B3LYP . . . . .	S-11
S2.4 Monomer vs WC Dimer Energies . . . . .	S-12
<b>S3 FrD-LVC Models Data</b>	<b>S-13</b>
S3.1 Diabatic Energies and Couplings . . . . .	S-13
S3.1.1 FC Point . . . . .	S-13
S3.1.2 Excited State Minima . . . . .	S-15
S3.2 Eigenvalues and Eigenvectors of Adiabatic FrD-LVC States . . . . .	S-19
S3.2.1 FC Point . . . . .	S-19
S3.2.2 Excited State Minima . . . . .	S-21
S3.3 Norm of Coupling Vector: FC Point . . . . .	S-23
S3.4 Adiabatic State Projection Convergence . . . . .	S-25
<b>S4 Additional Dynamics Results</b>	<b>S-28</b>
S4.1 Deuterated Calculations . . . . .	S-28
S4.2 Diabatic Potential Energies . . . . .	S-29
S4.3 Diabatic Potential Couplings . . . . .	S-33
S4.4 Electronic Only Dynamics . . . . .	S-36
S4.5 G→C(CT)1 Diabatic Energy Gap Dependence . . . . .	S-37
<b>S5 Additional Absorption Spectra</b>	<b>S-38</b>
S5.1 Comparison To Experimental Absorption Spectrum in Chloroform . . . . .	S-38
<b>S6 6-31+G(d,p) Basis Set Test</b>	<b>S-39</b>
S6.1 Single Point Energies . . . . .	S-39
S6.2 ωB97X-D 6-31+G(d,p) FrD-LVC Model . . . . .	S-40

## S1 Additional Numerical Details

### S1.1 Diabatization Scheme in TD-DFT

As discussed in the Methods section in the main text, we define the reference states of the fragments  $|\mathbf{R}^{\text{ frags}}(0)\rangle$  and overlap matrix between these reference states and the adiabatic states of the multichromophore (MC) at reference geometry  $\mathbf{S}(0) = \langle \mathbf{R}^{\text{ frags}}(0) | \mathbf{a}^{\text{ MC}}(0) \rangle$  and displaced geometry  $\mathbf{S}(\Delta_\alpha) = \langle \mathbf{R}^{\text{ frags}}(0) | \mathbf{a}^{\text{ MC}}(\Delta_\alpha) \rangle$  within the framework of TD-DFT. For this, we use transition densities, which in super-operator notation may be written as:

$$|\rho\rangle\rangle = \sum_{ir} X_{ir} |\Phi_r\rangle\langle\Phi_i| + \sum_{ir} Y_{ir} |\Phi_i\rangle\langle\Phi_r| \quad (\text{S1})$$

where  $X_{ir}$  and  $Y_{ir}$  are the response vectors,  $\Phi$  the molecular orbitals (MOs), and  $i$  and  $j$  will be used to signify occupied MOs, and  $r$  and  $s$  virtual MOs. The response vectors are output by standard electronic structure packages, typically written on the basis of molecular orbitals, and allow the local excitation reference states to be defined as equivalent to local excitations of individual fragments. Charge transfer reference states may be defined as single orbital transitions between an occupied orbital on one fragment, and a virtual orbital on another. Of course, a user-defined local excitation (such as HOMO-LUMO transition) is also possible.

Proceeding with the derivation of the overlap matrix, the inner product between two transition densities for states  $A$  and  $B$  may be written as a trace operation over the MOs

$$\begin{aligned} \langle\langle \rho^A | \rho^B \rangle\rangle &= \text{Tr}_\Phi \left[ \left( \sum_{ir} X_{ir}^A |\Phi_i\rangle\langle\Phi_r| - \sum_{ir} Y_{ir}^A |\Phi_r\rangle\langle\Phi_i| \right) \right. \\ &\quad \left. \left( \sum_{js} X_{js}^B |\Phi_s\rangle\langle\Phi_j| + \sum_{js} Y_{js}^B |\Phi_j\rangle\langle\Phi_s| \right) \right]. \end{aligned} \quad (\text{S2})$$

If the above was computed for two states of the same system with the same MOs, it would be equal to the Kronecker delta  $\delta_{AB}$ . However, if state  $A$  is a reference state of the fragments, and state  $B$  is an adiabatic state of the MC, then in general MOs of the fragments will not be orthogonal to the MOs of the MC either at the reference or displaced geometry. For the remainder of the derivation we illustrate how  $\mathbf{S}(\Delta_\alpha)$  is calculated, and then state how  $\mathbf{S}(0)$  is obtained at the end. Eq. S2 can be expanded as

$$\begin{aligned} \langle\langle \rho^A(0) | \rho^B(\Delta_\alpha) \rangle\rangle &= \text{Tr}_{\Phi(0)} \left[ \sum_{ir,js} X_{ir}^{A,0} X_{js}^{B,\Delta_\alpha} |\Phi_i^{\text{ frags}}(0)\rangle\langle\Phi_r^{\text{ frags}}(0)| \Phi_s^{\text{ MC}}(\Delta_\alpha)\rangle\langle\Phi_j^{\text{ MC}}(\Delta_\alpha)| \right] \\ &\quad - \text{Tr}_{\Phi(0)} \left[ \sum_{ir,js} Y_{ir}^{A,0} Y_{js}^{B,\Delta_\alpha} |\Phi_r^{\text{ frags}}(0)\rangle\langle\Phi_i^{\text{ frags}}(0)| \Phi_j^{\text{ MC}}(\Delta_\alpha)\rangle\langle\Phi_s^{\text{ MC}}(\Delta_\alpha)| \right] \\ &\quad + \text{Tr}_{\Phi(0)} \left[ \sum_{ir,js} X_{ir}^{A,0} Y_{js}^{B,\Delta_\alpha} |\Phi_i^{\text{ frags}}(0)\rangle\langle\Phi_r^{\text{ frags}}(0)| \Phi_j^{\text{ MC}}(\Delta_\alpha)\rangle\langle\Phi_s^{\text{ MC}}(\Delta_\alpha)| \right] \\ &\quad - \text{Tr}_{\Phi(0)} \left[ \sum_{ir,js} Y_{ir}^{A,0} X_{js}^{B,\Delta_\alpha} |\Phi_r^{\text{ frags}}(0)\rangle\langle\Phi_i^{\text{ frags}}(0)| \Phi_s^{\text{ MC}}(\Delta_\alpha)\rangle\langle\Phi_j^{\text{ MC}}(\Delta_\alpha)| \right]. \end{aligned} \quad (\text{S3})$$

where the MOs have been explicitly labelled as to whether they are those of the fragments or the MC, and labels have been added for the reference (0) and displaced ( $\Delta_\alpha$ ) geometries. Performing the trace operations

yields:

$$\begin{aligned}
\langle\langle \rho^A(0) | \rho^B(\Delta_\alpha) \rangle\rangle &= \sum_{ir,js} X_{ir}^{A,0} X_{js}^{B,\Delta_\alpha} \langle \Phi_r^{\text{frags}}(0) | \Phi_s^{\text{MC}}(\Delta_\alpha) \rangle \langle \Phi_j^{\text{MC}}(\Delta_\alpha) | \Phi_i^{\text{frags}}(0) \rangle \\
&\quad - \sum_{ir,js} Y_{ir}^{A,0} Y_{js}^{B,\Delta_\alpha} \langle \Phi_i^{\text{frags}}(0) | \Phi_j^{\text{MC}}(\Delta_\alpha) \rangle \langle \Phi_s^{\text{MC}}(\Delta_\alpha) | \Phi_r^{\text{frags}}(0) \rangle \\
&\quad + \sum_{ir,js} X_{ir}^{A,0} Y_{js}^{B,\Delta_\alpha} \langle \Phi_r^{\text{frags}}(0) | \Phi_j^{\text{MC}}(\Delta_\alpha) \rangle \langle \Phi_s^{\text{MC}}(\Delta_\alpha) | \Phi_i^{\text{frags}}(0) \rangle \\
&\quad - \sum_{ir,js} Y_{ir}^{A,0} X_{js}^{B,\Delta_\alpha} \langle \Phi_i^{\text{frags}}(0) | \Phi_s^{\text{MC}}(\Delta_\alpha) \rangle \langle \Phi_j^{\text{MC}}(\Delta_\alpha) | \Phi_r^{\text{frags}}(0) \rangle
\end{aligned} \tag{S4}$$

As the MOs are calculated at different geometries, we will now move in a basis of atomic orbitals (AOs) by introducing two resolutions of identity for the AOs of the MC at the reference geometry  $\sum_\lambda |\phi_\lambda^{\text{MC}}(0)\rangle \langle \phi_\lambda^{\text{MC}}(0)|$  and  $\sum_\mu |\phi_\mu^{\text{MC}}(0)\rangle \langle \phi_\mu^{\text{MC}}(0)|$  and two at displaced geometry  $\sum_\nu |\phi_\nu^{\text{MC}}(\Delta_\alpha)\rangle \langle \phi_\nu^{\text{MC}}(\Delta_\alpha)|$  and  $\sum_\sigma |\phi_\sigma^{\text{MC}}(\Delta_\alpha)\rangle \langle \phi_\sigma^{\text{MC}}(\Delta_\alpha)|$ . The response vectors in the AO basis are then

$$X_{\mu\lambda}^{\text{AO},A,0} = \sum_{ir} X_{ir}^{A,0} \langle \phi_\lambda^{\text{MC}}(0) | \Phi_r^{\text{frags}}(0) \rangle \langle \Phi_i^{\text{frags}}(0) | \phi_\mu^{\text{MC}}(0) \rangle \tag{S5}$$

$$Y_{\mu\lambda}^{\text{AO},A,0} = \sum_{ir} Y_{ir}^{A,0} \langle \phi_\mu^{\text{MC}}(0) | \Phi_i^{\text{frags}}(0) \rangle \langle \Phi_r^{\text{frags}}(0) | \phi_\lambda^{\text{MC}}(0) \rangle \tag{S6}$$

$$X_{\sigma\nu}^{\text{AO},B,\Delta_\alpha} = \sum_{js} X_{js}^{B,\Delta_\alpha} \langle \phi_\nu^{\text{MC}}(\Delta_\alpha) | \Phi_s^{\text{MC}}(\Delta_\alpha) \rangle \langle \Phi_j^{\text{MC}}(\Delta_\alpha) | \phi_\sigma^{\text{MC}}(\Delta_\alpha) \rangle \tag{S7}$$

$$Y_{\sigma\nu}^{\text{AO},B,\Delta_\alpha} = \sum_{js} Y_{js}^{B,\Delta_\alpha} \langle \phi_\sigma^{\text{MC}}(\Delta_\alpha) | \Phi_j^{\text{MC}}(\Delta_\alpha) \rangle \langle \Phi_s^{\text{MC}}(\Delta_\alpha) | \phi_\nu^{\text{MC}}(\Delta_\alpha) \rangle \tag{S8}$$

For the calculation of overlaps in Eq. S5 and S6 between the AOs of the MC and MOs of the fragments at reference geometry, given that the AOs of the fragments will be the same as the AOs for the MC at the same geometry, and that the linear combination of atomic orbitals is written as

$$|\Phi_r^{\text{frags}}(0)\rangle = \sum_\eta c_{r\eta}^{\text{frags}} |\phi_\eta^{\text{frags}}(0)\rangle \tag{S9}$$

where  $c_{r\eta}$  are the MO coefficients, then the overlap is

$$\begin{aligned}
\langle \phi_\lambda^{\text{MC}}(0) | \Phi_r^{\text{frags}}(0) \rangle &= \sum_\eta c_{r\eta}^{\text{frags}} \langle \phi_\lambda^{\text{MC}}(0) | \phi_\eta^{\text{frags}}(0) \rangle \\
&= \sum_\eta c_{r\eta}^{\text{frags}} \langle \phi_\lambda^{\text{MC}}(0) | \phi_\eta^{\text{MC}}(0) \rangle .
\end{aligned} \tag{S10}$$

Then, in the AO basis the trace over the transition density scalar product is:

$$\begin{aligned} \langle\langle\rho^A(0)|\rho^B(\Delta_\alpha)\rangle\rangle &= \sum_{\mu\lambda,\sigma\nu} X_{\mu\lambda}^{\text{AO},A,0} X_{\sigma\nu}^{\text{AO},B,\Delta_\alpha} \langle\phi_\lambda^{\text{MC}}(0)|\phi_\nu^{\text{MC}}(\Delta_\alpha)\rangle \langle\phi_\sigma^{\text{MC}}(\Delta_\alpha)|\phi_\mu^{\text{MC}}(0)\rangle \\ &\quad - \sum_{\mu\lambda,\sigma\nu} Y_{\mu\lambda}^{\text{AO},A,0} Y_{\sigma\nu}^{\text{AO},B,\Delta_\alpha} \langle\phi_\mu^{\text{MC}}(0)|\phi_\sigma^{\text{MC}}(\Delta_\alpha)\rangle \langle\phi_\nu^{\text{MC}}(\Delta_\alpha)|\phi_\lambda^{\text{MC}}(0)\rangle \\ &\quad + \sum_{\mu\lambda,\sigma\nu} X_{\mu\lambda}^{\text{AO},A,0} Y_{\sigma\nu}^{\text{AO},B,\Delta_\alpha} \langle\phi_\lambda^{\text{MC}}(0)|\phi_\sigma^{\text{MC}}(\Delta_\alpha)\rangle \langle\phi_\nu^{\text{MC}}(\Delta_\alpha)|\phi_\mu^{\text{MC}}(0)\rangle \\ &\quad - \sum_{\mu\lambda,\sigma\nu} Y_{\mu\lambda}^{\text{AO},A,0} X_{\sigma\nu}^{\text{AO},B,\Delta_\alpha} \langle\phi_\mu^{\text{MC}}(0)|\phi_\nu^{\text{MC}}(\Delta_\alpha)\rangle \langle\phi_\sigma^{\text{MC}}(\Delta_\alpha)|\phi_\lambda^{\text{MC}}(0)\rangle \end{aligned} \quad (\text{S11})$$

Finally, following Ref. 1 and our previous works,<sup>2-6</sup> we make the approximation that the AO overlap at two different but similar geometries of the MC can be approximated by one at the reference geometry to get

$$\begin{aligned} \langle\langle\rho^A(0)|\rho^B(\Delta_\alpha)\rangle\rangle &\simeq \sum_{\mu\lambda,\sigma\nu} X_{\mu\lambda}^{\text{AO},A,0} X_{\sigma\nu}^{\text{AO},B,\Delta_\alpha} \langle\phi_\lambda^{\text{MC}}(0)|\phi_\nu^{\text{MC}}(0)\rangle \langle\phi_\sigma^{\text{MC}}(0)|\phi_\mu^{\text{MC}}(0)\rangle \\ &\quad - \sum_{\mu\lambda,\sigma\nu} Y_{\mu\lambda}^{\text{AO},A,0} Y_{\sigma\nu}^{\text{AO},B,\Delta_\alpha} \langle\phi_\mu^{\text{MC}}(0)|\phi_\sigma^{\text{MC}}(0)\rangle \langle\phi_\nu^{\text{MC}}(0)|\phi_\lambda^{\text{MC}}(0)\rangle \\ &\quad + \sum_{\mu\lambda,\sigma\nu} X_{\mu\lambda}^{\text{AO},A,0} Y_{\sigma\nu}^{\text{AO},B,\Delta_\alpha} \langle\phi_\lambda^{\text{MC}}(0)|\phi_\sigma^{\text{MC}}(0)\rangle \langle\phi_\nu^{\text{MC}}(0)|\phi_\mu^{\text{MC}}(0)\rangle \\ &\quad - \sum_{\mu\lambda,\sigma\nu} Y_{\mu\lambda}^{\text{AO},A,0} X_{\sigma\nu}^{\text{AO},B,\Delta_\alpha} \langle\phi_\mu^{\text{MC}}(0)|\phi_\nu^{\text{MC}}(0)\rangle \langle\phi_\sigma^{\text{MC}}(0)|\phi_\lambda^{\text{MC}}(0)\rangle \\ &= \rho_{XX}^{AB}(\Delta_\alpha) - \rho_{YY}^{AB}(\Delta_\alpha) + \rho_{XY}^{AB}(\Delta_\alpha) - \rho_{YX}^{AB}(\Delta_\alpha). \end{aligned} \quad (\text{S12})$$

So the elements of the overlap matrix  $\mathbf{S}(\Delta_\alpha)$  are

$$S_{AB}(\Delta_\alpha) = \rho_{XX}^{AB}(\Delta_\alpha) - \rho_{YY}^{AB}(\Delta_\alpha) + \rho_{XY}^{AB}(\Delta_\alpha) - \rho_{YX}^{AB}(\Delta_\alpha). \quad (\text{S13})$$

Note that we can take advantage of the symmetry of the AO overlap matrix in Eq. S12 to efficiently calculate the overlap in terms of matrix multiplications and a final sum over two indeces, reducing the problem from a  $\mathcal{O}(N^4)$  cost to  $\mathcal{O}(N^3)$ . This immediately becomes apparent by re-arranging the order of multiplication in Eq. S12 in the following manner, using the shorthand notation  $S_{\lambda,\nu}^{\text{AO,MC},0}$  to represent  $\langle\phi_\lambda^{\text{MC}}(0)|\phi_\nu^{\text{MC}}(0)\rangle$ , and noting that  $S_{\lambda,\nu}^{\text{AO,MC},0} = S_{\nu,\lambda}^{\text{AO,MC},0}$

$$\rho_{XX}^{AB}(\Delta_\alpha) = \sum_{\mu\lambda,\sigma\nu} X_{\mu\lambda}^{\text{AO},A,0} S_{\mu,\sigma}^{\text{AO,MC},0} X_{\sigma\nu}^{\text{AO},B,\Delta_\alpha} S_{\nu,\lambda}^{\text{AO,MC},0} \quad (\text{S14})$$

$$\rho_{YY}^{AB}(\Delta_\alpha) = \sum_{\mu\lambda,\sigma\nu} Y_{\mu\lambda}^{\text{AO},A,0} S_{\mu,\sigma}^{\text{AO,MC},0} Y_{\sigma\nu}^{\text{AO},B,\Delta_\alpha} S_{\nu,\lambda}^{\text{AO,MC},0} \quad (\text{S15})$$

$$\rho_{XY}^{AB}(\Delta_\alpha) = \sum_{\mu\lambda,\sigma\nu} X_{\mu\lambda}^{\text{AO},A,0} S_{\lambda,\sigma}^{\text{AO,MC},0} X_{\sigma\nu}^{\text{AO},B,\Delta_\alpha} S_{\nu,\mu}^{\text{AO,MC},0} \quad (\text{S16})$$

$$\rho_{YX}^{AB}(\Delta_\alpha) = \sum_{\mu\lambda,\sigma\nu} Y_{\mu\lambda}^{\text{AO},A,0} S_{\lambda,\sigma}^{\text{AO,MC},0} X_{\sigma\nu}^{\text{AO},B,\Delta_\alpha} S_{\nu,\mu}^{\text{AO,MC},0} \quad (\text{S17})$$

The final three terms in each of the above equations are evaluated by matrix multiplication, removing the  $\sigma$  and  $\nu$  indeces, and leaving a final sum over the  $\mu$  and  $\lambda$  indeces. This is the more computationally efficient method of calculating the overlap matrix compared to our previous applications mentioned in the main text. The calculation of  $S(0)$  can also utilise Eqs. S13 - S17, simply by replacing the response vectors at displaced geometries  $X_{\sigma\nu}^{\text{AO},B,\Delta_\alpha}$  and  $Y_{\sigma\nu}^{\text{AO},B,\Delta_\alpha}$  by those at the reference geometry  $X_{\sigma\nu}^{\text{AO},B,0}$  and  $Y_{\sigma\nu}^{\text{AO},B,0}$ .

Since we define CT states including only the excitation response vector, for a balanced treatment of LE and CT states we use the Tamm-Dancoff approximation so that we take only the  $\rho_{XX}^{AB}$  element of the inner product, and the elements of the overlap matrix are

$$S_{AB} = \rho_{XX}^{AB}. \quad (\text{S18})$$

## S1.2 Absorption Spectra

The transition dipole moments of the diabatic states at the reference geometry  $\mu[d(0)]$  may be obtained by applying the transformation matrix  $D(0)$  to the diagonal matrix of adiabatic transition dipole moments of the MC at reference geometry  $\mu[a^{\text{MC}}(0)]$

$$\mu[d(0)] = D(0)^T \mu[a^{\text{MC}}(0)] D(0). \quad (\text{S19})$$

This is the same procedure as the calculation of the diabatic Hamiltonian matrix in Eq. 7 in the main text, and we also adopted this in Ref. 7 to calculate diabatic transition dipole moments.

Then, the absorption spectra  $\epsilon(\omega)$  at zero Kelvin, can be expressed in a TD framework as:

$$\begin{aligned} \epsilon(\omega) &= \frac{2\pi\omega N_A}{3000 \times \ln 10 \times \hbar c_0 (4\pi\epsilon_0)} \sum_{ji} \int_{-\infty}^{\infty} dt e^{i\omega t - \Gamma t^2} \langle \mathbf{0}; d_j | \mu_{gj}^d e^{-i\hat{H}t/\hbar} \mu_{ig}^d | d_i; \mathbf{0} \rangle \\ &= \sum_i \epsilon_{ii}(\omega) + \sum_{i,j \neq i} \epsilon_{ij}(\omega) = \epsilon^{\text{auto}}(\omega) + \epsilon^{\text{cross}}(\omega) \end{aligned} \quad (\text{S20})$$

where  $N_A$  is Avogadro's number,  $c_0$  is the speed of light in vacuo,  $\epsilon_0$  is the vacuum permittivity and we introduced a quadratic damping ruled by a parameter  $\Gamma$ , corresponding to a Gaussian broadening in the frequency domain. We represent the diabatic transition dipole moments obtained by the transformation in Eq. S19 with the shorthand  $\mu_{gj}^d$  for the transition from ground state  $g$  to diabatic state  $d_j$ . The diabatic transition dipole moment is considered independent of the nuclear coordinates (Condon approximation), and the ground-vibrational state of the ground electronic state is represented by  $\mathbf{0}$  and its energy is set to zero.

The auto ( $\epsilon^{\text{auto}}$ ) and cross ( $\epsilon^{\text{cross}}$ ) correlation functions are obtained by numerical propagation in time under the effect of the FrD-LVC Hamiltonian of the doorway states  $|d_j; \mathbf{0}\rangle$  obtained by a vertical excitation of the vibrational state  $\mathbf{0}$  to the bright diabatic states (i.e. for which  $\mu_{ig}$  is non vanishing). Then, the vibronic absorption spectrum is obtained by Fourier transform of the sum of the correlations functions weighted by the scalar products of the diabatic transition dipoles (as reported in Equation S20). Cross-correlations functions usually have a very small effect and have been neglected.<sup>2,6</sup>

## S2 Electronic Structure Details and Data

### S2.1 Natural Transition Orbitals

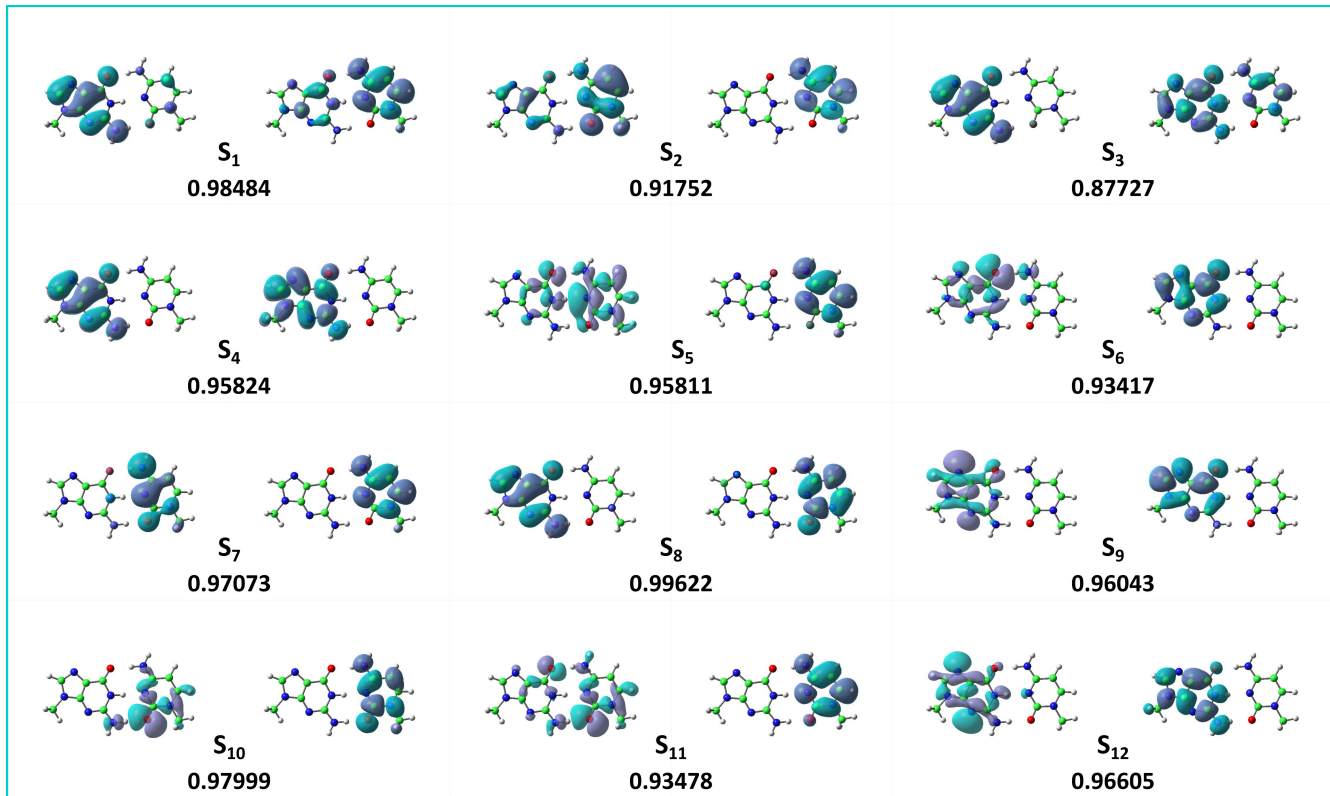


Figure S1: Frontier NTOs (occupied on the left and virtual on the right) and their eigenvalues for the first 12 singlet states of GC in the gas phase at ground state geometry  $C_s$  symmetry using the CAM-B3LYP functional and 6-31G(d) basis set with an isovalue 0.02 for all orbitals.

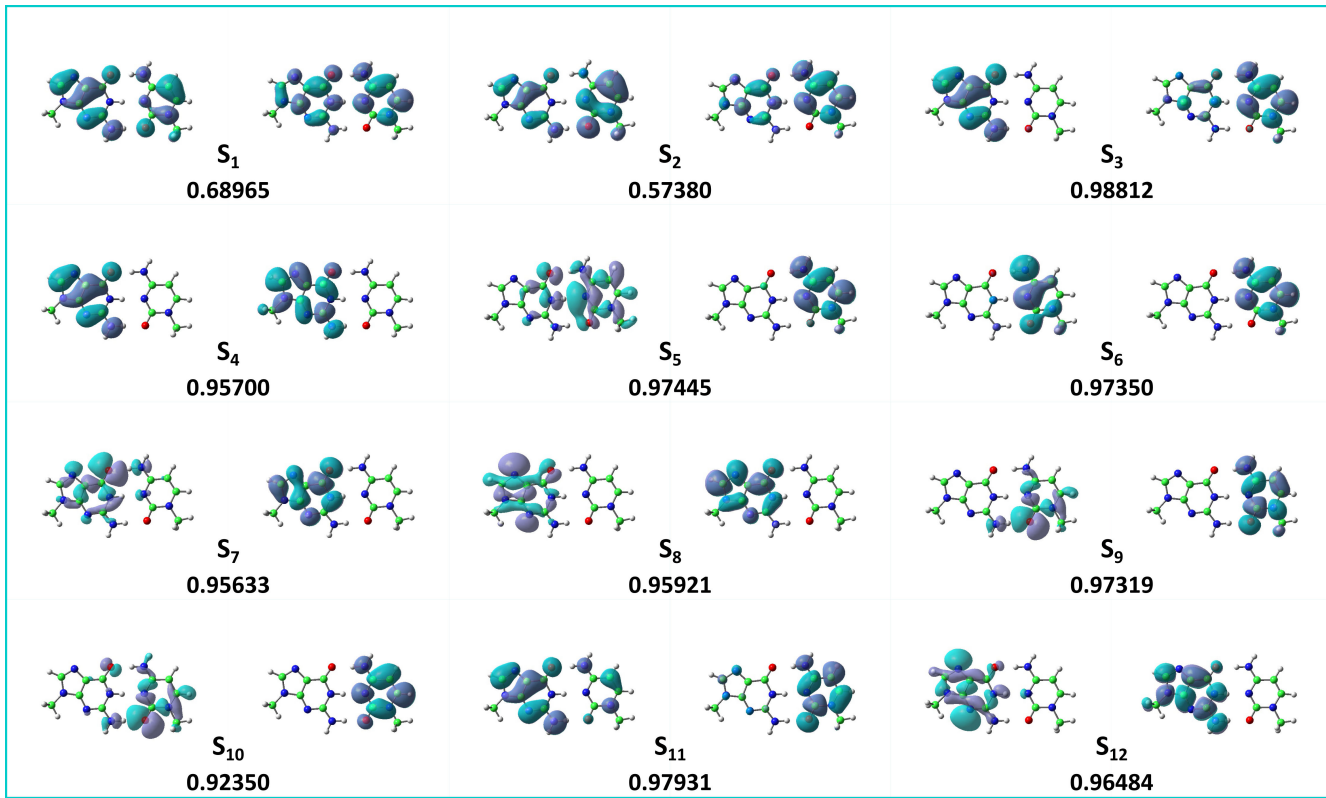


Figure S2: Frontier NTOs (occupied on the left and virtual on the right) and their eigenvalues for the first 12 singlet states of GC in the gas phase at ground state geometry  $C_s$  symmetry using the  $\omega$ B97X-D functional and 6-31G(d) basis set with an isovalue 0.02 for all orbitals.

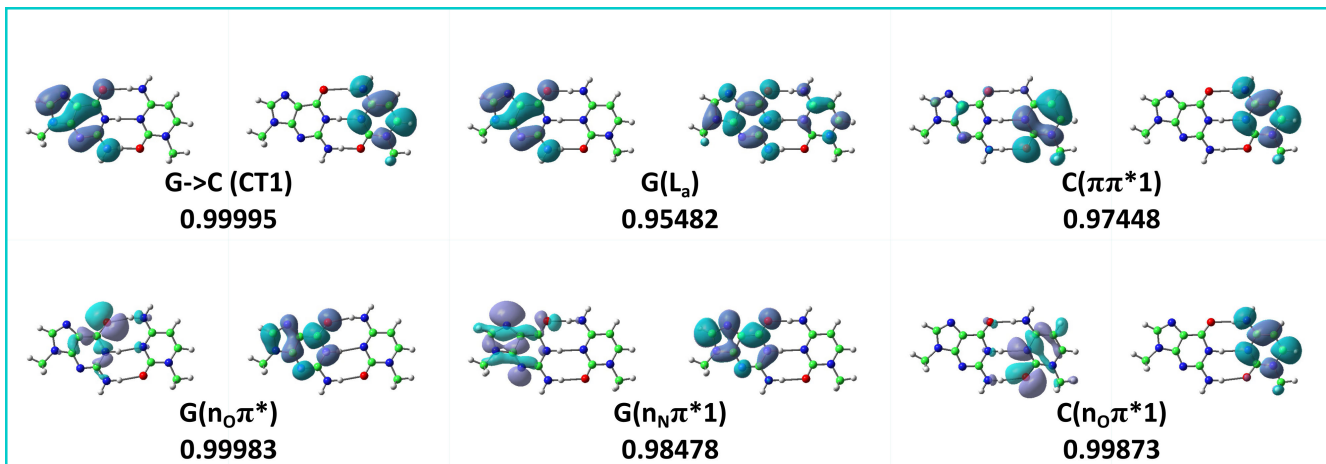


Figure S3: Frontier NTOs (occupied on the left and virtual on the right) and their eigenvalues for the adiabatic planar excited state minima of GC in the gas phase using the CAM-B3LYP functional and 6-31G(d) basis set with an isovalue 0.02 for all orbitals.

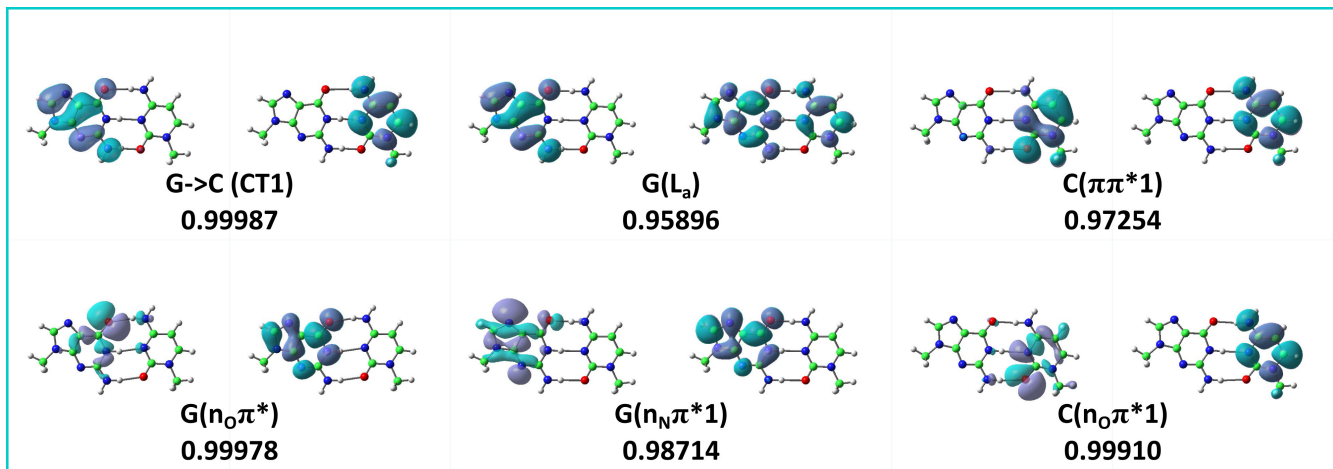


Figure S4: Frontier NTOs (occupied on the left and virtual on the right) and their eigenvalues for the adiabatic planar excited state minima of GC in the gas phase using the  $\omega$ B97X-D functional and 6-31G(d) basis set with an isovalue 0.02 for all orbitals.

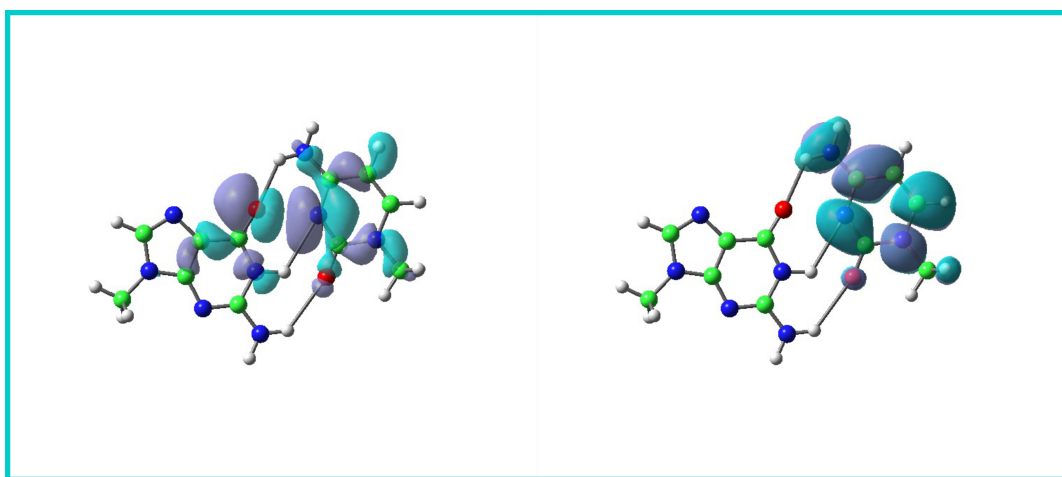


Figure S5: Frontier NTOs (occupied on the left and virtual on the right) for the  $S_5$  adiabatic planar excited state minimum of GC in the gas phase using the CAM-B3LYP functional and 6-31G(d) basis set with an isovalue 0.02 for the orbitals.

## S2.2 Adiabatic TD-DFT Minima Calculation Details

We succeeded in optimizing the minima of  $G \rightarrow C(CT)1$ ,  $C(\pi\pi^*1)$ ,  $G(L_a)$ ,  $G(n_O\pi^*)$ ,  $G(n_N\pi^*1)$  and  $C(n_O\pi^*1)$  states (see NTOs in Figures S3 and S4). For the  $G \rightarrow C(CT)1$  optimisation, the hydrogen bonded N-H bond lengths on G had to be frozen at the same distance as in the  $S_0$  minimum, to prevent the H atom being transferred to C. The vertical energy gaps between the  $G \rightarrow C(CT)1$  TD-DFT minima and  $S_0$  are 2.92 eV with CAM-B3LYP/6-31G(d), and 3.37 eV with  $\omega$ B97X-D/6-31G(d). Geometry optimizations of the adiabatic states corresponding to  $C(\pi\pi^*2)$ ,  $G(L_b)$ ,  $G(n_N\pi^*2)$ ,  $C(n_O\pi^*2)$  and  $G \rightarrow C(CT)2$  states lead to the minima of the corresponding lower lying excited state ( $C(\pi\pi^*1)$ ,  $G(L_a)$ ,  $G(n_N\pi^*1)$ ,  $C(n_O\pi^*1)$ , and  $G \rightarrow C(CT)1$ ). Finally, attempted geometry optimization of the adiabatic state corresponding to  $C(n_N\pi^*)$  ( $S_5$  at the FC position) with CAM-B3LYP instead leads to a state which appears to resemble the  $n\pi^*$ -CT state with ‘wobble GC’ configuration recently put forward in Ref.8 (see Figure S5). Given this different hydrogen bonding arrangement, we do not consider this state in the present work. However it is interesting to note that we also observe a similar CT character of this state, with 0.32 e<sup>-</sup> of charge transferred from G to C in this state relative to the ground state, according to Mulliken Population Analysis. Attempted geometry optimisation of the  $C(n_N\pi^*)$  ( $S_5$ ) state with  $\omega$ B97X-D lead to a similar structure, but then was unable to be converged.

### S2.3 Normal Modes CAM-B3LYP

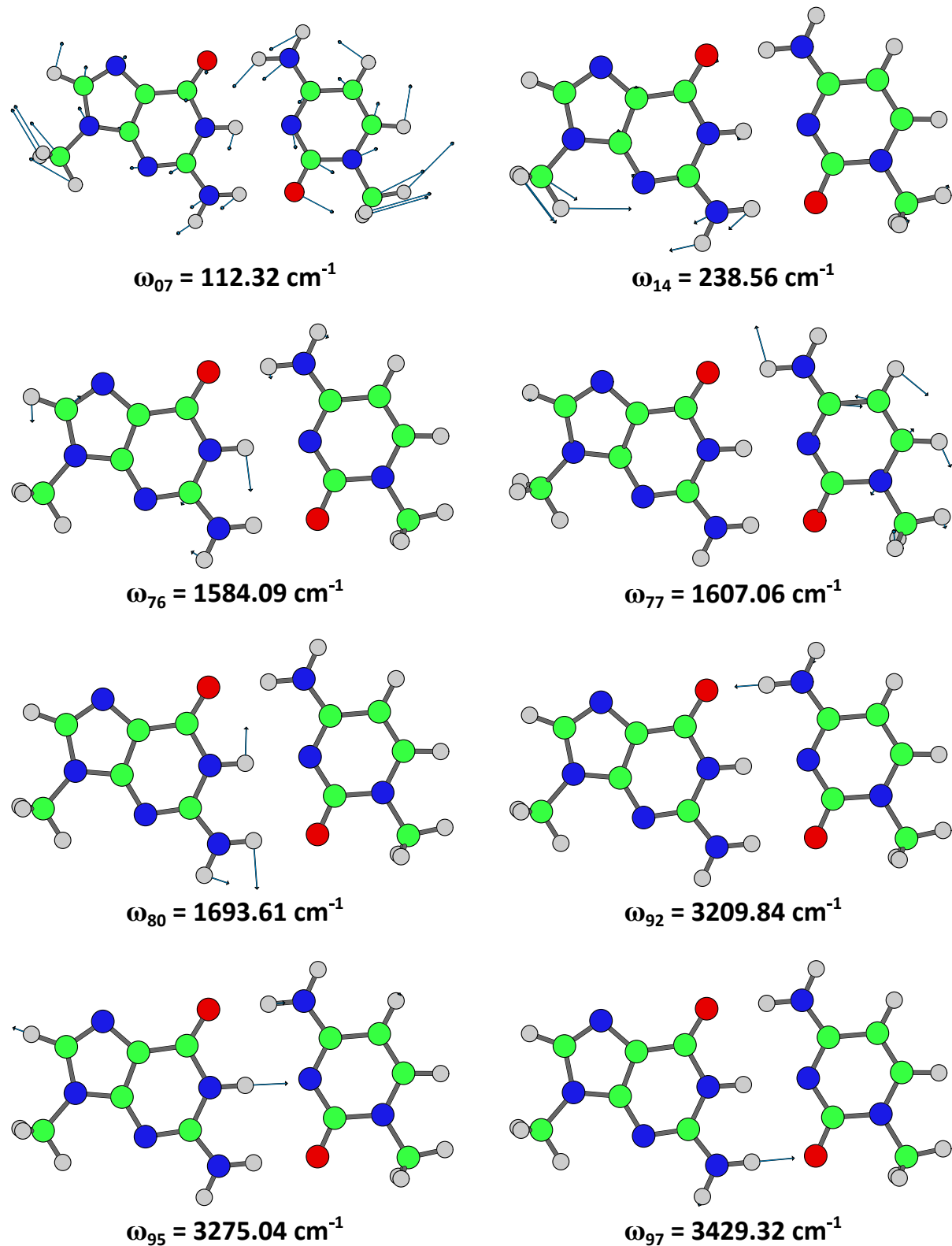


Figure S6: Normal modes shown in Figure 5 in the main text, at the CAM-B3LYP/6-31G(d) level of theory.

## S2.4 Monomer vs WC Dimer Energies

Table S1: TD-DFT excitation energies (eV) and oscillator strengths (in parentheses) of the 9-methylguanine 1-methylcytosine WC pair and individual monomers in  $C_s$  symmetry at their respective equilibrium geometries, obtained with the CAM-B3LYP and  $\omega$ B97X-D functionals and 6-31G(d) basis set.

Char.	CAM-B3LYP		$\omega$ B97X-D	
	G/C Mon.	GC Dimer	G/C Mon.	GC Dimer
C( $\pi\pi^*$ )	5.09 (0.090)	5.27 (0.114)	5.07 (0.090)	5.28 (0.140)
G(L <sub>a</sub> )	5.33 (0.154)	5.31 (0.087)	5.32 (0.151)	5.21 (0.071)
G(L <sub>b</sub> )	5.80 (0.271)	5.69 (0.403)	5.78 (0.273)	5.69 (0.402)
C(n <sub>N</sub> $\pi^*$ )	5.40 (0.001)	5.79 (0.001)	5.36 (0.001)	5.77 (0.001)
G(n <sub>O</sub> $\pi^*$ )	5.63 (0.000)	5.93 (0.000)	5.64 (0.000)	5.93 (0.000)
C( $\pi\pi^*2$ )	6.07 (0.153)	5.93 (0.126)	6.03 (0.148)	5.90 (0.112)
G(n <sub>N</sub> $\pi^*1$ )	6.51 (0.005)	6.44 (0.004)	6.50 (0.004)	6.43 (0.003)
C(n <sub>O</sub> $\pi^*1$ )	5.95 (0.001)	6.45 (0.000)	5.93 (0.001)	6.46 (0.000)
C(n <sub>O</sub> $\pi^*2$ )	6.18 (0.000)	6.60 (0.000)	6.14 (0.000)	6.56 (0.000)
G(n <sub>N</sub> $\pi^*2$ )	6.63 (0.001)	6.71 (0.000)	6.60 (0.000)	6.70 (0.000)

## S3 FrD-LVC Models Data

### S3.1 Diabatic Energies and Couplings

#### S3.1.1 FC Point

Table S2: Diabatic energies ( $E_{ii}^d(0)$ ) and electronic couplings ( $E_{ij}^d(0)$ ) of bright  $\pi\pi^*$  and CT states of GC in  $C_s$  symmetry at equilibrium geometry from the FrD-LVC CAM-B3LYP and  $\omega$ B97X-D 6-31G(d) 12 state models (eV)

	$G \rightarrow C(CT)1$	$C(\pi\pi^*1)$	$G(L_a)$	$G(L_b)$	$C(\pi\pi^*2)$	$G \rightarrow C(CT)2$
<u>CAM-B3LYP</u>						
$G \rightarrow C(CT)1$	5.169					
$C(\pi\pi^*1)$	0.022	5.325				
$G(L_a)$	0.065	0.002	5.425			
$G(L_b)$	0.038	-0.020	-0.171	5.658		
$C(\pi\pi^*2)$	-0.039	0.160	0.053	0.041	5.915	
$G \rightarrow C(CT)2$	-0.061	-0.004	-0.027	0.035	0.003	6.393
<u><math>\omega</math>B97X-D</u>						
$G \rightarrow C(CT)1$	5.540					
$C(\pi\pi^*1)$	0.023	5.311				
$G(L_a)$	0.067	0.002	5.418			
$G(L_b)$	0.037	-0.018	-0.176	5.650		
$C(\pi\pi^*2)$	-0.036	0.155	0.052	0.037	5.886	
$G \rightarrow C(CT)2$	-0.097	-0.004	-0.027	0.033	0.005	6.673

Table S3: Diabatic energies ( $E_{ii}^d(0)$ ) and electronic couplings ( $E_{ij}^d(0)$ ) of  $n\pi^*$  states of GC in  $C_s$  symmetry at equilibrium geometry from the FrD-LVC CAM-B3LYP and  $\omega$ B97X-D 6-31G(d) 12 state models (eV)

	$C(n_N\pi^*)$	$G(n_O\pi^*)$	$G(n_N\pi^*1)$	$C(n_O\pi^*1)$	$C(n_O\pi^*2)$	$G(n_N\pi^*2)$
<u>CAM-B3LYP</u>						
$C(n_N\pi^*)$	5.921					
$G(n_O\pi^*)$	0.005	5.935				
$G(n_N\pi^*1)$	-0.002	-0.048	6.496			
$C(n_O\pi^*1)$	0.013	-0.002	0.001	6.543		
$C(n_O\pi^*2)$	0.004	0.001	-0.001	-0.093	6.554	
$G(n_N\pi^*2)$	-0.001	-0.019	-0.112	0.001	0.001	6.731
<u><math>\omega</math>B97X-D</u>						
$C(n_N\pi^*)$	5.884					
$G(n_O\pi^*)$	0.005	5.948				
$G(n_N\pi^*1)$	-0.003	-0.053	6.470			
$C(n_O\pi^*1)$	0.019	-0.002	0.001	6.526		
$C(n_O\pi^*2)$	0.005	0.000	-0.001	-0.059	6.530	
$G(n_N\pi^*2)$	0.001	-0.022	-0.114	0.000	0.001	6.728

### S3.1.2 Excited State Minima

Table S4: Diabatic energies ( $V_{ii}^d(\mathbf{q})$ ) for each of the states in the 12 state FrD-LVC models at the minima of every A' (i.e.  $\pi\pi^*$  and CT) diabatic state ( $\mathbf{q}_{\min}^{d,i}$ ). Parametrized by CAM-B3LYP and  $\omega$ B97X-D with 6-31G(d) basis set.

In Min Diab. State →	G→C(CT)1	C( $\pi\pi^*1$ )	G(L <sub>a</sub> )	G(L <sub>b</sub> )	C( $\pi\pi^*2$ )	G→C(CT)2
<u>CAM-B3LYP</u>						
G→C(CT)1	3.938	4.923	5.130	5.023	4.970	4.695
C( $\pi\pi^*1$ )	5.920	4.935	5.661	5.667	5.196	6.628
G(L <sub>a</sub> )	6.287	5.821	5.094	5.379	5.858	6.272
G(L <sub>b</sub> )	6.409	6.057	5.610	5.325	6.081	6.417
C( $\pi\pi^*2$ )	6.516	5.746	6.248	6.241	5.485	7.255
G→C(CT)2	5.960	6.897	6.381	6.295	6.973	5.203
C( $n_N\pi^*$ )	6.732	5.986	6.258	6.289	5.999	7.174
G( $n_O\pi^*$ )	7.280	6.335	6.156	6.147	6.384	7.187
G( $n_N\pi^*1$ )	7.546	6.896	6.601	6.384	6.921	7.532
C( $n_O\pi^*1$ )	7.114	6.142	6.888	6.895	6.551	7.837
C( $n_O\pi^*2$ )	7.412	6.522	6.895	6.889	6.651	7.455
G( $n_N\pi^*2$ )	7.875	7.134	6.541	6.880	7.155	7.839
<u><math>\omega</math>B97X-D</u>						
G→C(CT)1	4.394	5.321	5.504	5.392	5.354	5.128
C( $\pi\pi^*1$ )	5.852	4.925	5.636	5.650	5.188	6.573
G(L <sub>a</sub> )	6.209	5.810	5.100	5.381	5.851	6.259
G(L <sub>b</sub> )	6.319	6.046	5.602	5.321	6.078	6.378
C( $\pi\pi^*2$ )	6.416	5.719	6.208	6.213	5.456	7.158
G→C(CT)2	6.270	7.184	6.695	6.593	7.238	5.536
C( $n_N\pi^*$ )	6.656	5.951	6.211	6.254	5.947	7.119
G( $n_O\pi^*$ )	7.207	6.347	6.154	6.161	6.393	7.152
G( $n_N\pi^*1$ )	7.450	6.863	6.571	6.355	6.897	7.471
C( $n_O\pi^*1$ )	6.964	6.013	6.855	6.872	6.431	7.877
C( $n_O\pi^*2$ )	7.418	6.591	6.857	6.861	6.737	7.307
G( $n_N\pi^*2$ )	7.758	7.127	6.511	6.873	7.158	7.772

Table S5: Diabatic energies ( $V_{ii}^d(\mathbf{q})$ ) for each of the states in the 12 state FrD-LVC models at the minima of every  $A''$  (i.e.  $n\pi^*$ ) diabatic state ( $\mathbf{q}_{\min}^{d,i}$ ). Parametrized by CAM-B3LYP and  $\omega$ B97X-D with 6-31G(d) basis set.

In Min Diab. State →	$C(n_N\pi^*)$	$G(n_O\pi^*)$	$G(n_N\pi^*1)$	$C(n_O\pi^*1)$	$C(n_O\pi^*2)$	$G(n_N\pi^*2)$
<u>CAM-B3LYP</u>						
$G \rightarrow C(CT)1$	5.329	5.716	5.554	5.397	5.414	5.599
$C(\pi\pi^*1)$	5.580	5.767	5.901	5.421	5.520	5.856
$G(L_a)$	6.011	5.748	5.765	6.327	6.053	5.422
$G(L_b)$	6.274	5.969	5.778	6.564	6.278	5.992
$C(\pi\pi^*2)$	6.143	6.366	6.475	6.380	6.199	6.427
$G \rightarrow C(CT)2$	7.036	6.887	6.805	7.385	6.721	6.828
$C(n_N\pi^*)$	5.341	6.345	6.501	6.459	6.785	6.430
$G(n_O\pi^*)$	6.507	5.503	6.349	6.857	6.570	6.311
$G(n_N\pi^*1)$	7.090	6.776	5.930	7.399	7.119	6.320
$C(n_O\pi^*1)$	6.773	7.010	7.124	5.655	6.258	7.077
$C(n_O\pi^*2)$	7.380	7.003	7.125	6.539	5.936	7.090
$G(n_N\pi^*2)$	7.303	7.022	6.603	7.636	7.367	6.214
<u><math>\omega</math>B97X-D</u>						
$G \rightarrow C(CT)1$	5.739	6.076	5.971	5.808	5.869	5.965
$C(\pi\pi^*1)$	5.566	5.748	5.916	5.388	5.574	5.866
$G(L_a)$	6.000	5.729	5.798	6.405	6.014	5.424
$G(L_b)$	6.265	5.957	5.803	6.643	6.239	6.008
$C(\pi\pi^*2)$	6.093	6.325	6.480	6.337	6.250	6.427
$G \rightarrow C(CT)2$	7.345	7.163	7.134	7.863	6.900	7.121
$C(n_N\pi^*)$	5.311	6.303	6.500	6.462	6.761	6.422
$G(n_O\pi^*)$	6.517	5.525	6.366	6.961	6.546	6.354
$G(n_N\pi^*1)$	7.062	6.714	5.873	7.458	7.060	6.304
$C(n_O\pi^*1)$	6.702	6.986	7.135	5.550	6.289	7.085
$C(n_O\pi^*2)$	7.394	6.963	7.130	6.682	5.943	7.087
$G(n_N\pi^*2)$	7.298	7.016	6.618	7.721	7.330	6.187

Table S6: Diabatic energies ( $V_{ii}^d(\mathbf{q})$ ) for each of the states in the 12 state FrD-LVC models at the TD-DFT adiabatic planar minima ( $\mathbf{q}_{\min}^{\text{ad},m}$ ) discussed in the main text. Parametrized by CAM-B3LYP and  $\omega$ B97X-D with 6-31G(d) basis set.

In Min Ad. State →	G→C(CT)1	C( $\pi\pi^*1$ )	G(L <sub>a</sub> )	G(n <sub>O</sub> $\pi^*$ )	G(n <sub>N</sub> $\pi^*1$ )	C(n <sub>O</sub> $\pi^*1$ )
<u>CAM-B3LYP</u>						
G→C(CT)1	4.038	4.844	4.898	6.087	5.821	5.591
C( $\pi\pi^*1$ )	5.716	4.951	5.504	6.084	6.103	5.548
G(L <sub>a</sub> )	6.109	5.826	5.180	6.007	5.983	6.668
G(L <sub>b</sub> )	6.252	6.057	5.559	6.245	5.989	6.903
C( $\pi\pi^*2$ )	6.334	5.743	6.101	6.668	6.671	6.351
G→C(CT)2	6.064	6.838	6.239	7.236	7.079	8.017
C(n <sub>N</sub> $\pi^*$ )	6.582	6.014	6.112	6.622	6.700	6.504
G(n <sub>O</sub> $\pi^*$ )	7.162	6.367	6.029	5.565	6.428	7.189
G(n <sub>N</sub> $\pi^*1$ )	7.388	6.908	6.526	7.035	6.020	7.740
C(n <sub>O</sub> $\pi^*1$ )	6.858	6.063	6.697	7.323	7.313	5.914
C(n <sub>O</sub> $\pi^*2$ )	7.133	6.424	6.769	7.321	7.320	6.802
G(n <sub>N</sub> $\pi^*2$ )	7.705	7.151	6.581	7.267	6.712	7.976
<u><math>\omega</math>B97X-D</u>						
G→C(CT)1	4.477	5.289	5.430	6.461	6.203	5.999
C( $\pi\pi^*1$ )	5.675	4.939	5.536	6.078	6.102	5.511
G(L <sub>a</sub> )	6.081	5.823	5.206	5.999	5.992	6.676
G(L <sub>b</sub> )	6.211	6.056	5.562	6.253	6.007	6.915
C( $\pi\pi^*2$ )	6.272	5.718	6.095	6.639	6.661	6.316
G→C(CT)2	6.360	7.145	6.640	7.523	7.359	8.323
C(n <sub>N</sub> $\pi^*$ )	6.514	5.980	6.127	6.594	6.680	6.579
G(n <sub>O</sub> $\pi^*$ )	7.121	6.368	6.028	5.592	6.449	7.225
G(n <sub>N</sub> $\pi^*1$ )	7.339	6.879	6.481	6.988	5.943	7.730
C(n <sub>O</sub> $\pi^*1$ )	6.723	5.954	6.735	7.314	7.311	5.701
C(n <sub>O</sub> $\pi^*2$ )	7.183	6.500	6.766	7.293	7.313	6.865
G(n <sub>N</sub> $\pi^*2$ )	7.627	7.143	6.581	7.281	6.722	7.990

Table S7:  $\pi\pi^*$ -CT, excitonic, and  $\pi\pi^*$  mixing couplings between diabatic states ( $V_{ij}^d(\mathbf{q})$ , eV) at the FC point (S<sub>0</sub> minimum column), and the G→C(CT)1, C( $\pi\pi^*1$ ) and L<sub>a</sub> adiabatic ( $q_{\min}^{ad,m}$ ) and diabatic ( $q_{\min}^{d,i}$ ) minima as predicted by the 12 state FrD-LVC models parametrized by CAM-B3LYP and ωB97X-D with 6-31G(d) basis set.

In Min. State →	S <sub>0</sub>	$q_{\min}^{ad,m}$			$q_{\min}^{d,i}$		
Coupling ↓	CAM-B3LYP						
G(L <sub>a</sub> ) : G→C(CT)1	0.065	0.066	0.057	0.065	0.069	0.057	0.065
G(L <sub>b</sub> ) : G→C(CT)1	0.038	0.014	0.031	0.033	0.014	0.032	0.034
C( $\pi\pi^*1$ ) : G→C(CT)1	0.022	0.038	0.022	0.025	0.045	0.021	0.020
C( $\pi\pi^*2$ ) : G→C(CT)1	-0.039	-0.005	-0.032	-0.035	-0.001	-0.033	-0.038
G(L <sub>a</sub> ) : C( $\pi\pi^*1$ )	0.002	0.002	0.000	0.003	0.002	-0.001	0.002
G(L <sub>a</sub> ) : C( $\pi\pi^*2$ )	0.053	0.049	0.049	0.053	0.048	0.049	0.054
G(L <sub>b</sub> ) : C( $\pi\pi^*1$ )	-0.020	-0.026	-0.024	-0.021	-0.027	-0.025	-0.021
G(L <sub>b</sub> ) : C( $\pi\pi^*2$ )	0.041	0.034	0.040	0.042	0.034	0.040	0.042
G(L <sub>a</sub> ) : G(L <sub>b</sub> )	-0.171	-0.018	-0.167	-0.201	-0.038	-0.169	-0.068
C( $\pi\pi^*1$ ) : C( $\pi\pi^*2$ )	0.160	0.031	0.025	0.148	0.045	0.063	0.164
Coupling ↓	ωB97X-D						
G(L <sub>a</sub> ) : G→C(CT)1	0.067	0.083	0.065	0.076	0.087	0.065	0.067
G(L <sub>b</sub> ) : G→C(CT)1	0.037	0.013	0.030	0.037	0.014	0.030	0.034
C( $\pi\pi^*1$ ) : G→C(CT)1	0.023	0.040	0.023	0.025	0.046	0.022	0.022
C( $\pi\pi^*2$ ) : G→C(CT)1	-0.036	-0.009	-0.030	-0.040	-0.007	-0.030	-0.036
G(L <sub>a</sub> ) : C( $\pi\pi^*1$ )	0.002	0.002	0.000	0.001	0.001	-0.001	0.000
G(L <sub>a</sub> ) : C( $\pi\pi^*2$ )	0.052	0.049	0.049	0.054	0.049	0.048	0.052
G(L <sub>b</sub> ) : C( $\pi\pi^*1$ )	-0.018	-0.022	-0.020	-0.020	-0.022	-0.021	-0.020
G(L <sub>b</sub> ) : C( $\pi\pi^*2$ )	0.037	0.029	0.035	0.041	0.029	0.035	0.038
G(L <sub>a</sub> ) : G(L <sub>b</sub> )	-0.176	-0.032	-0.181	-0.232	-0.044	-0.179	-0.072
C( $\pi\pi^*1$ ) : C( $\pi\pi^*2$ )	0.155	0.034	0.025	0.149	0.044	0.054	0.160

## S3.2 Eigenvalues and Eigenvectors of Adiabatic FrD-LVC States

### S3.2.1 FC Point

Table S8: Eigenvalues (eV) of A' adiabatic FrD-LVC states and corresponding normalised eigenvectors showing the contribution of the  $\pi\pi^*$  and CT diabatic states from the 12 state FrD-LVC models of GC in  $C_s$  symmetry at the FC point. Parametrized by CAM-B3LYP and  $\omega$ B97X-D with 6-31G(d) basis set.

	CAM-B3LYP					
Adiabatic states →	$S_1$	$S_2$	$S_3$	$S_4$	$S_7$	$S_8$
Eigenval. (eV) →	5.125	5.291	5.360	5.746	5.963	6.399
Eigenvec. ↓						
G→C(CT)1	0.898	0.266	0.346	0.012	-0.031	-0.050
C( $\pi\pi^*1$ )	-0.208	0.934	-0.157	-0.050	0.239	-0.004
G( $L_a$ )	-0.318	0.025	0.822	-0.464	0.071	-0.040
G( $L_b$ )	-0.185	0.059	0.421	0.882	0.071	0.054
C( $\pi\pi^*2$ )	0.117	-0.229	-0.041	-0.018	0.965	0.010
G→C(CT)2	0.041	0.017	0.028	-0.066	-0.011	0.996
	$\omega$ B97X-D					
Adiabatic states →	$S_1$	$S_2$	$S_3$	$S_4$	$S_6$	$S_{11}$
Eigenval. (eV) →	5.248	5.313	5.557	5.744	5.932	6.683
Eigenvec. ↓						
G→C(CT)1	-0.234	-0.203	0.945	0.023	-0.054	-0.085
C( $\pi\pi^*1$ )	0.778	-0.574	0.083	-0.040	0.237	-0.004
G( $L_a$ )	0.445	0.707	0.275	-0.470	0.071	-0.031
G( $L_b$ )	0.276	0.356	0.130	0.880	0.059	0.035
C( $\pi\pi^*2$ )	-0.254	0.055	0.005	-0.009	0.965	0.009
G→C(CT)2	-0.010	-0.011	0.085	-0.043	-0.012	0.995

Table S9: Eigenvalues (eV) of A'' adiabatic FrD-LVC states and corresponding normalised eigenvectors showing the contribution of the  $n\pi^*$  diabatic states from the 12 state FrD-LVC models of GC in  $C_s$  symmetry at the FC point. Parametrized by CAM-B3LYP and  $\omega$ B97X-D with 6-31G(d) basis set.

	CAM-B3LYP					
Adiabatic states →	$S_5$	$S_6$	$S_9$	$S_{10}$	$S_{11}$	$S_{12}$
Eigenval. (eV) →	5.918	5.932	6.455	6.457	6.642	6.776
Eigenvec. ↓						
$C(n_N\pi^*)$	0.920	0.392	0.023	0.003	-0.008	0.000
$G(n_O\pi^*)$	-0.391	0.915	0.033	-0.094	0.002	0.000
$G(n_N\pi^*1)$	-0.032	0.087	-0.312	0.870	-0.003	-0.371
$C(n_O\pi^*1)$	-0.021	-0.007	0.685	0.244	-0.686	0.001
$C(n_O\pi^*2)$	-0.009	-0.004	0.645	0.236	0.727	0.005
$G(n_N\pi^*2)$	-0.013	0.035	-0.128	0.346	-0.005	0.929
	$\omega$ B97X-D					
Adiabatic states →	$S_5$	$S_7$	$S_8$	$S_9$	$S_{10}$	$S_{12}$
Eigenval. (eV) →	5.883	5.941	6.433	6.470	6.587	6.771
Eigenvec. ↓						
$C(n_N\pi^*)$	0.996	0.083	-0.005	0.029	-0.013	0.002
$G(n_O\pi^*)$	-0.083	0.990	-0.118	-0.003	0.003	-0.002
$G(n_N\pi^*1)$	-0.004	0.109	0.929	0.012	-0.002	-0.354
$C(n_O\pi^*1)$	-0.030	0.000	-0.013	0.718	-0.695	-0.004
$C(n_O\pi^*2)$	-0.011	-0.001	-0.004	0.695	0.719	0.007
$G(n_N\pi^*2)$	-0.004	0.044	0.351	0.002	-0.009	0.935

### S3.2.2 Excited State Minima

Table S10: Eigenvalues (eV) of adiabatic FrD-LVC states in diabatic minima geometries ( $q_{\min}^{d,i}$ ) shown in Table 3 in the main text, and the corresponding normalised eigenvectors. From 12 state FrD-LVC models parametrized by CAM-B3LYP and  $\omega$ B97X-D functionals and 6-31G(d) basis set.

In Min Diab. State →	G→C(CT)1	C( $\pi\pi^*1$ )	G(L <sub>a</sub> )	G(n <sub>O</sub> $\pi^*$ )	G(n <sub>N</sub> $\pi^*1$ )	C(n <sub>O</sub> $\pi^*1$ )
Eigenvec. ↓	CAM-B3LYP					
Eigenval. (eV) →	3.934	4.948	5.030	5.501	5.811	5.572
G→C(CT)1	-0.999	0.607	-0.596	0.000	0.000	0.000
C( $\pi\pi^*1$ )	0.023	0.793	0.038	0.000	0.000	0.000
G(L <sub>a</sub> )	0.030	-0.037	0.788	0.000	0.000	0.000
G(L <sub>b</sub> )	0.006	-0.004	0.134	0.000	0.000	0.000
C( $\pi\pi^*2$ )	-0.002	-0.036	-0.063	0.000	0.000	0.000
G→C(CT)2	0.016	0.011	-0.016	0.000	0.000	0.000
C(n <sub>N</sub> $\pi^*$ )	0.000	0.000	0.000	0.005	-0.002	0.095
G(n <sub>O</sub> $\pi^*$ )	0.000	0.000	0.000	-0.999	0.351	0.000
G(n <sub>N</sub> $\pi^*1$ )	0.000	0.000	0.000	0.021	0.905	0.000
C(n <sub>O</sub> $\pi^*1$ )	0.000	0.000	0.000	-0.001	0.000	-0.959
C(n <sub>O</sub> $\pi^*2$ )	0.000	0.000	0.000	0.000	0.000	0.269
G(n <sub>N</sub> $\pi^*2$ )	0.000	0.000	0.000	0.033	0.239	0.001
Eigenvec. ↓	$\omega$ B97X-D					
Eigenval. (eV) →	4.388	4.920	5.074	5.523	5.746	5.475
G→C(CT)1	-0.998	-0.063	-0.170	0.000	0.000	0.000
C( $\pi\pi^*1$ )	0.032	0.995	0.029	0.000	0.000	0.000
G(L <sub>a</sub> )	0.048	0.014	0.972	0.000	0.000	0.000
G(L <sub>b</sub> )	0.009	0.025	0.149	0.000	0.000	0.000
C( $\pi\pi^*2$ )	-0.006	-0.071	-0.059	0.000	0.000	0.000
G→C(CT)2	-0.007	-0.001	0.003	0.000	0.000	0.000
C(n <sub>N</sub> $\pi^*$ )	0.000	0.000	0.000	0.006	-0.001	0.063
G(n <sub>O</sub> $\pi^*$ )	0.000	0.000	0.000	-0.999	0.342	0.000
G(n <sub>N</sub> $\pi^*1$ )	0.000	0.000	0.000	0.021	0.912	0.000
C(n <sub>O</sub> $\pi^*1$ )	0.000	0.000	0.000	-0.001	0.000	-0.970
C(n <sub>O</sub> $\pi^*2$ )	0.000	0.000	0.000	0.000	0.000	0.235
G(n <sub>N</sub> $\pi^*2$ )	0.000	0.000	0.000	0.030	0.228	0.000

Table S11: Eigenvalues (eV) of adiabatic FrD-LVC states in TD-DFT adiabatic minima geometries ( $q_{\min}^{\text{ad},m}$ ) shown in Table 3 in the main text, and the corresponding normalised eigenvectors. From 12 state FrD-LVC models parametrized by CAM-B3LYP and  $\omega$ B97X-D functionals and 6-31G(d) basis set.

In Min Ad. State →	G→C(CT)1	C( $\pi\pi^*1$ )	G(L <sub>a</sub> )	G(n <sub>O</sub> $\pi^*$ )	G(n <sub>N</sub> $\pi^*1$ )	C(n <sub>O</sub> $\pi^*1$ )
Eigenvec. ↓	CAM-B3LYP					
Eigenval. (eV) →	4.033	4.955	5.114	5.559	5.790	5.556
G→C(CT)1	0.999	0.197	0.320	0.000	0.000	0.000
C( $\pi\pi^*1$ )	-0.022	0.980	0.015	0.000	0.000	0.000
G(L <sub>a</sub> )	-0.033	-0.009	0.869	0.000	0.000	0.000
G(L <sub>b</sub> )	-0.007	0.015	0.372	0.000	0.000	0.000
C( $\pi\pi^*2$ )	0.003	-0.023	-0.053	0.000	0.000	0.000
G→C(CT)2	-0.026	0.000	0.033	0.000	0.000	0.000
C(n <sub>N</sub> $\pi^*$ )	0.000	0.000	0.000	0.004	0.004	0.232
G(n <sub>O</sub> $\pi^*$ )	0.000	0.000	0.000	-0.998	-0.328	0.000
G(n <sub>N</sub> $\pi^*1$ )	0.000	0.000	0.000	0.043	-0.867	0.000
C(n <sub>O</sub> $\pi^*1$ )	0.000	0.000	0.000	-0.001	-0.001	-0.875
C(n <sub>O</sub> $\pi^*2$ )	0.000	0.000	0.000	0.000	0.000	0.424
G(n <sub>N</sub> $\pi^*2$ )	0.000	0.000	0.000	0.052	-0.374	0.002
Eigenvec. ↓	$\omega$ B97X-D					
Eigenval. (eV) →	4.471	4.936	5.065	5.586	5.730	5.481
G→C(CT)1	-0.998	0.071	-0.237	0.000	0.000	0.000
C( $\pi\pi^*1$ )	0.034	-0.996	0.055	0.000	0.000	0.000
G(L <sub>a</sub> )	0.052	-0.012	0.865	0.000	0.000	0.000
G(L <sub>b</sub> )	0.009	-0.023	0.431	0.000	0.000	0.000
C( $\pi\pi^*2$ )	-0.007	0.036	-0.079	0.000	0.000	0.000
G→C(CT)2	-0.004	0.000	-0.008	0.000	0.000	0.000
C(n <sub>N</sub> $\pi^*$ )	0.000	0.000	0.000	-0.005	0.002	0.129
G(n <sub>O</sub> $\pi^*$ )	0.000	0.000	0.000	0.998	-0.324	0.000
G(n <sub>N</sub> $\pi^*1$ )	0.000	0.000	0.000	-0.049	-0.883	0.000
C(n <sub>O</sub> $\pi^*1$ )	0.000	0.000	0.000	0.001	-0.001	-0.929
C(n <sub>O</sub> $\pi^*2$ )	0.000	0.000	0.000	0.000	0.000	0.346
G(n <sub>N</sub> $\pi^*2$ )	0.000	0.000	0.000	-0.049	-0.339	0.000

### S3.3 Norm of Coupling Vector: FC Point

Table S12: Norm of coupling vector  $\sqrt{\lambda_{ij} \cdot \lambda_{ij}}$  of GC in  $C_s$  symmetry at equilibrium geometry from the FrD-LVC CAM-B3LYP/6-31G(d) 12 state model

	G→C(CT)1	C( $\pi\pi^*1$ )	G( $L_a$ )	G( $L_b$ )	C( $\pi\pi^*2$ )	G→C(CT)2
G→C(CT)1	0.608					
C( $\pi\pi^*1$ )	0.008	0.364				
G( $L_a$ )	0.012	0.005	0.327			
G( $L_b$ )	0.010	0.005	0.183	0.342		
C( $\pi\pi^*2$ )	0.012	0.171	0.006	0.008	0.383	
G→C(CT)2	0.239	0.001	0.012	0.007	0.003	0.560
C( $n_N\pi^*$ )	0.030	0.116	0.005	0.005	0.100	0.005
G( $n_O\pi^*$ )	0.003	0.002	0.032	0.042	0.012	0.002
G( $n_N\pi^*1$ )	0.006	0.001	0.040	0.131	0.002	0.007
C( $n_O\pi^*1$ )	0.037	0.102	0.007	0.003	0.084	0.025
C( $n_O\pi^*2$ )	0.022	0.051	0.007	0.002	0.054	0.046
G( $n_N\pi^*2$ )	0.002	0.002	0.141	0.039	0.003	0.003
	C( $n_N\pi^*$ )	G( $n_O\pi^*$ )	G( $n_N\pi^*1$ )	C( $n_O\pi^*1$ )	C( $n_O\pi^*2$ )	G( $n_N\pi^*2$ )
C( $n_N\pi^*$ )	0.369					
G( $n_O\pi^*$ )	0.003	0.412				
G( $n_N\pi^*1$ )	0.002	0.093	0.406			
C( $n_O\pi^*1$ )	0.136	0.001	0.001	0.586		
C( $n_O\pi^*2$ )	0.090	0.001	0.001	0.285	0.496	
G( $n_N\pi^*2$ )	0.005	0.078	0.209	0.003	0.002	0.373

Table S13: Norm of coupling vector  $\sqrt{\lambda_{ij} \cdot \lambda_{ij}}$  of GC in  $C_s$  symmetry at equilibrium geometry from the FrD-LVC  $\omega$ B97X-D 12 state model

	G→C(CT)1	C( $\pi\pi^*1$ )	G(L <sub>a</sub> )	G(L <sub>b</sub> )	C( $\pi\pi^*2$ )	G→C(CT)2
G→C(CT)1	0.591					
C( $\pi\pi^*1$ )	0.008	0.363				
G(L <sub>a</sub> )	0.013	0.005	0.321			
G(L <sub>b</sub> )	0.010	0.004	0.182	0.340		
C( $\pi\pi^*2$ )	0.010	0.165	0.005	0.007	0.382	
G→C(CT)2	0.227	0.002	0.011	0.007	0.004	0.546
C( $n_N\pi^*$ )	0.034	0.113	0.005	0.003	0.100	0.005
G( $n_O\pi^*$ )	0.003	0.002	0.033	0.044	0.011	0.001
G( $n_N\pi^*1$ )	0.002	0.001	0.029	0.131	0.002	0.003
C( $n_O\pi^*1$ )	0.047	0.106	0.007	0.001	0.092	0.024
C( $n_O\pi^*2$ )	0.022	0.039	0.007	0.002	0.047	0.062
G( $n_N\pi^*2$ )	0.004	0.002	0.142	0.035	0.004	0.003
	C( $n_N\pi^*$ )	G( $n_O\pi^*$ )	G( $n_N\pi^*1$ )	C( $n_O\pi^*1$ )	C( $n_O\pi^*2$ )	G( $n_N\pi^*2$ )
C( $n_N\pi^*$ )	0.368					
G( $n_O\pi^*$ )	0.003	0.411				
G( $n_N\pi^*1$ )	0.002	0.103	0.415			
C( $n_O\pi^*1$ )	0.146	0.001	0.001	0.611		
C( $n_O\pi^*2$ )	0.090	0.000	0.001	0.261	0.485	
G( $n_N\pi^*2$ )	0.003	0.080	0.211	0.001	0.001	0.382

### S3.4 Adiabatic State Projection Convergence

In Tables S14 and S15 we show the convergence of the FrD projection of the A' and A'' reference states, with respect to the number of adiabatic states projected onto. This is illustrated with the diabatic energies  $E_{ii}^d(0)$  and constant couplings  $E_{ij}^d(0)$  obtained after projection onto 20, 30 and 40 adiabatic states from  $\omega$ B97X-D/6-31G(d) calculations at the reference geometry. The energies show only small differences ( $\sim < 0.05$  eV) and similarly the couplings also only show small differences ( $\sim < 0.01$  eV).

In addition, it is worthy to note that we can monitor the quality of the projection with the matrix  $M = SS^T$ . In the case that the reference states span the same subspace as the adiabatic states, we will have a complete projection and this matrix  $M$  will be equal to the identity matrix. Therefore, the diagonal values  $M_{ii}$  being close to 1 indicate that we have projected onto a sufficient number of adiabatic states, whilst at the same time values much less than 1 (e.g.  $< 0.8$ ) indicate we have not projected onto enough. In Fig. S7 we show these diagonal elements  $M_{ii}$  for each of the 12 reference diabatic states, as a function of the number of  $\omega$ B97X-D/6-31G(d) adiabatic states projected onto at the reference geometry.

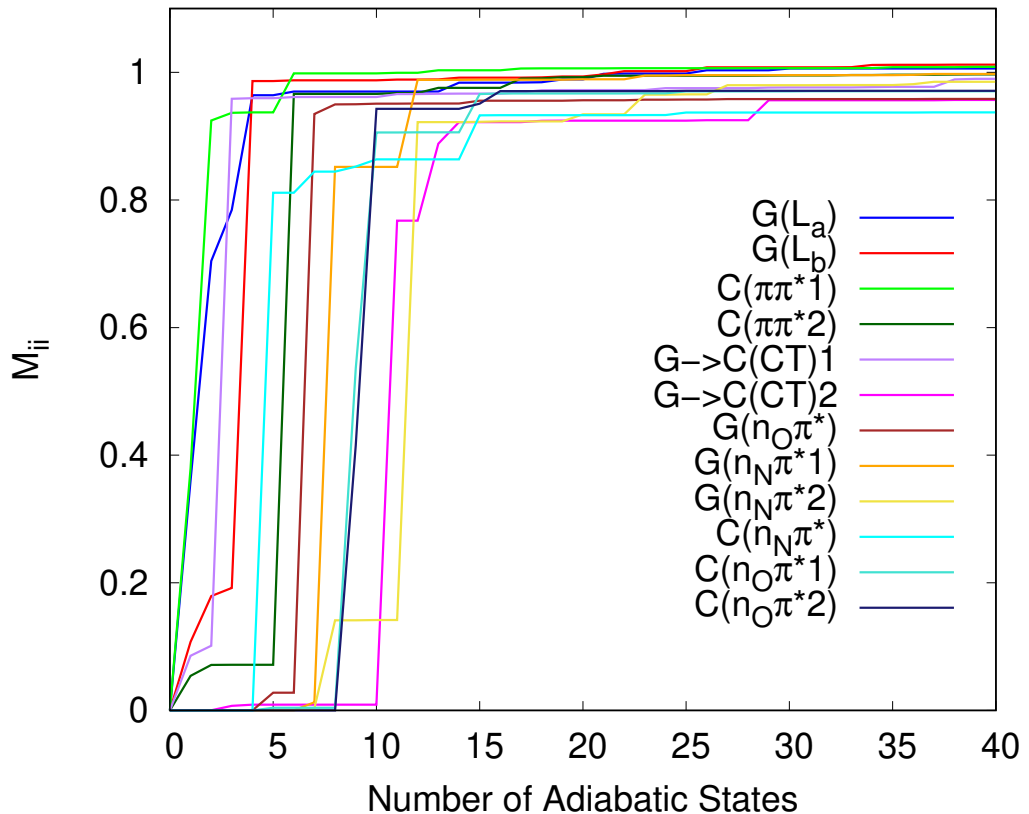


Figure S7: Diagonal elements of the matrix  $M = SS^T$  versus the number of adiabatic states  $|a^{MC}\rangle$  in the overlap matrix  $S = \langle R^{\text{frags}} | a^{MC} \rangle$  for each of the reference diabatic states  $|R^{\text{frags}}\rangle$ . Calculated using  $\omega$ B97X-D/6-31G(d) at the reference geometry.

Table S14: Diabatic energies ( $E_{ii}^d(0)$ ) and electronic couplings ( $E_{ij}^d(0)$ ) of bright  $\pi\pi^*$  and CT states of GC in  $C_s$  symmetry at equilibrium geometry from 12 state FrD projections onto different numbers of adiabatic states calculated by  $\omega$ B97X-D/6-31G(d) (eV)

	$G \rightarrow C(CT)1$	$C(\pi\pi^*1)$	$G(L_a)$	$G(L_b)$	$C(\pi\pi^*2)$	$G \rightarrow C(CT)2$
<u>20 States</u>						
$G \rightarrow C(CT)1$	5.486					
$C(\pi\pi^*1)$	0.024	5.303				
$G(L_a)$	0.065	0.001	5.378			
$G(L_b)$	0.036	-0.019	-0.175	5.610		
$C(\pi\pi^*2)$	-0.041	0.159	0.047	0.034	5.877	
$G \rightarrow C(CT)2$	-0.094	-0.004	-0.028	0.035	-0.003	6.622
<u>30 States</u>						
$G \rightarrow C(CT)1$	5.496					
$C(\pi\pi^*1)$	0.024	5.304				
$G(L_a)$	0.066	0.001	5.418			
$G(L_b)$	0.037	-0.019	-0.178	5.638		
$C(\pi\pi^*2)$	-0.041	0.158	0.053	0.039	5.882	
$G \rightarrow C(CT)2$	-0.104	-0.004	-0.027	0.034	0.004	6.672
<u>40 States</u>						
$G \rightarrow C(CT)1$	5.540					
$C(\pi\pi^*1)$	0.023	5.311				
$G(L_a)$	0.067	0.002	5.418			
$G(L_b)$	0.037	-0.018	-0.176	5.650		
$C(\pi\pi^*2)$	-0.036	0.155	0.052	0.037	5.886	
$G \rightarrow C(CT)2$	-0.097	-0.004	-0.027	0.033	0.005	6.673

Table S15: Diabatic energies ( $E_{ii}^d(0)$ ) and electronic couplings ( $E_{ij}^d(0)$ ) of  $n\pi^*$  states of GC in  $C_s$  symmetry at equilibrium geometry from 12 state FrD projections onto different numbers of adiabatic states calculated by  $\omega$ B97X-D 6-31G(d) (eV)

	$C(n_N\pi^*)$	$G(n_O\pi^*)$	$G(n_N\pi^*1)$	$C(n_O\pi^*1)$	$C(n_O\pi^*2)$	$G(n_N\pi^*2)$
<u>20 States</u>						
$C(n_N\pi^*)$	5.875					
$G(n_O\pi^*)$	0.006	5.943				
$G(n_N\pi^*1)$	-0.001	-0.052	6.459			
$C(n_O\pi^*1)$	0.025	-0.002	0.000	6.521		
$C(n_O\pi^*2)$	0.003	0.001	0.000	-0.057	6.530	
$G(n_N\pi^*2)$	0.009	-0.033	-0.096	-0.005	0.003	6.665
<u>30 States</u>						
$C(n_N\pi^*)$	5.884					
$G(n_O\pi^*)$	0.005	5.946				
$G(n_N\pi^*1)$	-0.002	-0.055	6.466			
$C(n_O\pi^*1)$	0.019	-0.002	0.001	6.526		
$C(n_O\pi^*2)$	0.005	0.000	-0.001	-0.059	6.530	
$G(n_N\pi^*2)$	0.000	-0.019	-0.108	0.000	0.001	6.718
<u>40 States</u>						
$C(n_N\pi^*)$	5.884					
$G(n_O\pi^*)$	0.005	5.948				
$G(n_N\pi^*1)$	-0.003	-0.053	6.470			
$C(n_O\pi^*1)$	0.019	-0.002	0.001	6.526		
$C(n_O\pi^*2)$	0.005	0.000	-0.001	-0.059	6.530	
$G(n_N\pi^*2)$	0.001	-0.022	-0.114	0.000	0.001	6.728

## S4 Additional Dynamics Results

### S4.1 Deuterated Calculations

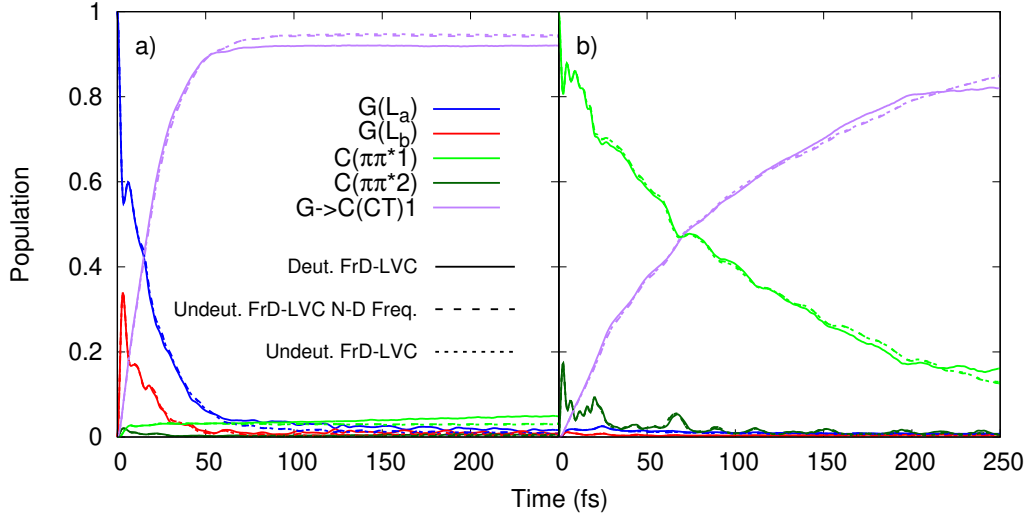


Figure S8: Populations for 5-state,  $A'$  vibrational mode GC FrD-LVC model built with the five central hydrogens deuterated (solid line), the FrD-LVC model from undeuterated GC in which the five N-H stretch frequencies are replaced with their deuterated value (dashed line), and the FrD-LVC model from undeuterated GC as in the main text Figure 3 (dotted line). Dynamics initiated on a)  $G(L_a)$  state and b)  $C(\pi\pi^*1)$  state. Parametrized by CAM-B3LYP/6-31G(d)

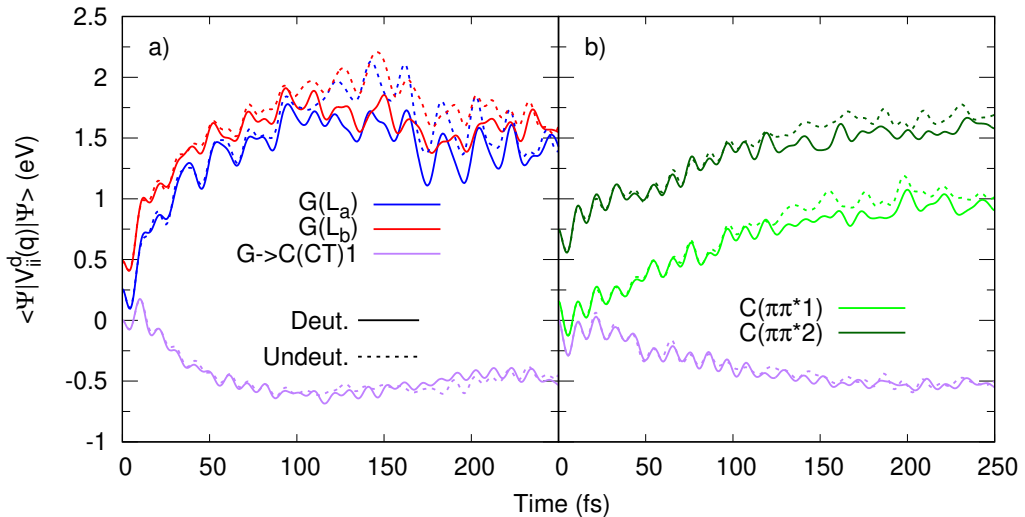


Figure S9: Expectation of diabatic state potential energies, ( $\langle \Psi | V_{ii}^d(q) | \Psi \rangle$ ) for the 5 state deuterated (solid line) and undeuterated (dashed line) FrD-LVC models. Dynamics initiated on a)  $G(L_a)$  state and b)  $C(\pi\pi^*1)$  state. Parametrized by CAM-B3LYP/6-31G(d). Shifted by  $-E_{CT1}^d(0) - 1/4 \sum_\alpha \omega_\alpha$  so that the  $G \rightarrow C(CT)1$  energy is 0 initially. Only the  $\pi\pi^*$  states on the base of initial photoexcitation are shown for simplicity.

## S4.2 Diabatic Potential Energies

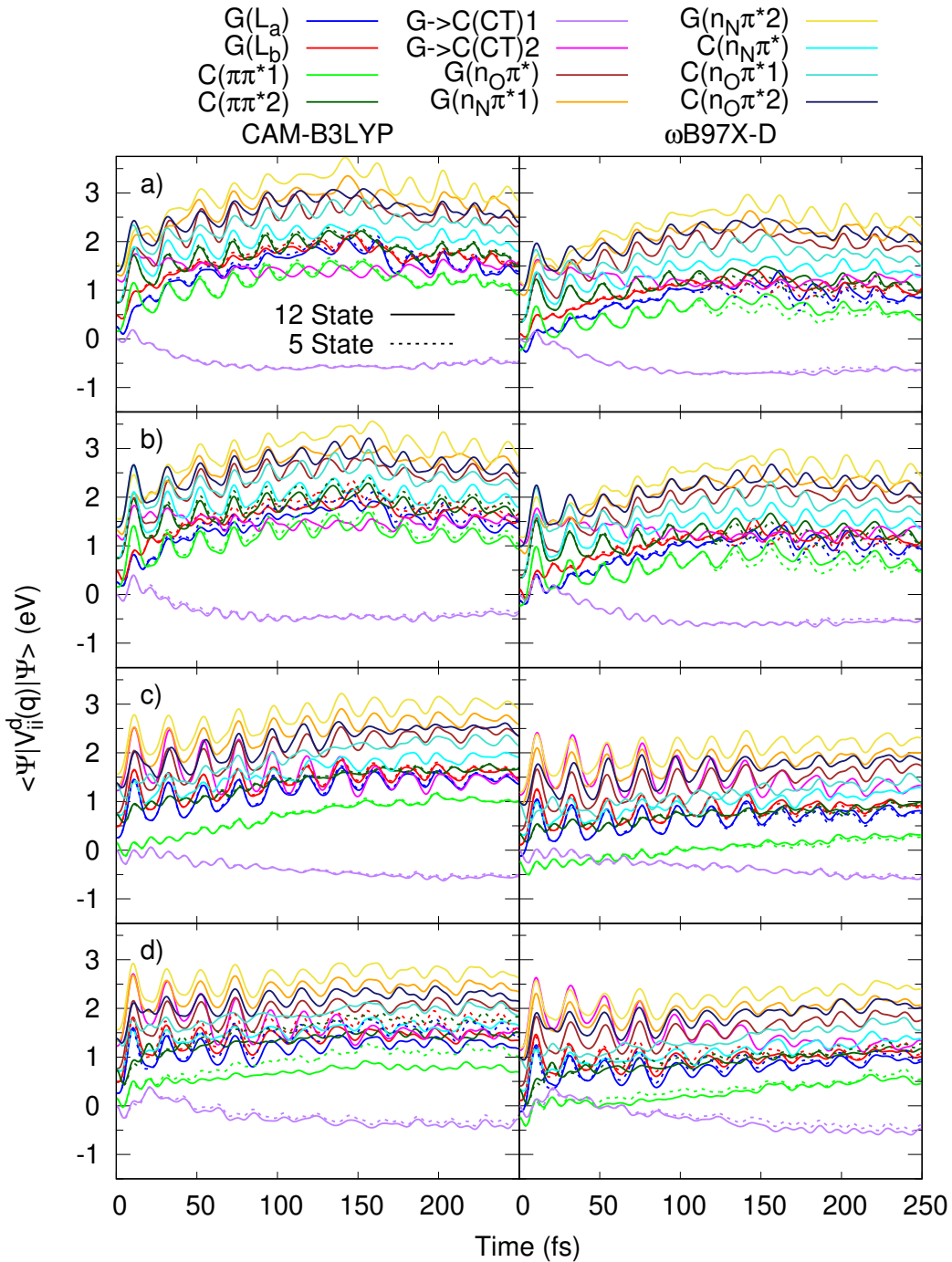


Figure S10: Expectation of diabatic state potential energies, ( $\langle \Psi | V_{ii}^d(q) | \Psi \rangle$ ) shifted by  $-E_{CT1}^d(0) - 1/4 \sum_\alpha \omega_\alpha$  so that the  $G \rightarrow C(CT)1$  energy is 0 initially. For the 12 state (solid lines) and 5 state (dotted lines) FrD-LVC models for GC, parametrized by left: CAM-B3LYP and right:  $\omega$ B97X-D with 6-31G(d) basis set, for dynamics initiated on a)  $G(L_a)$ , b)  $G(L_b)$ , c)  $C(\pi\pi^*1)$  and d)  $C(\pi\pi^*2)$  states.

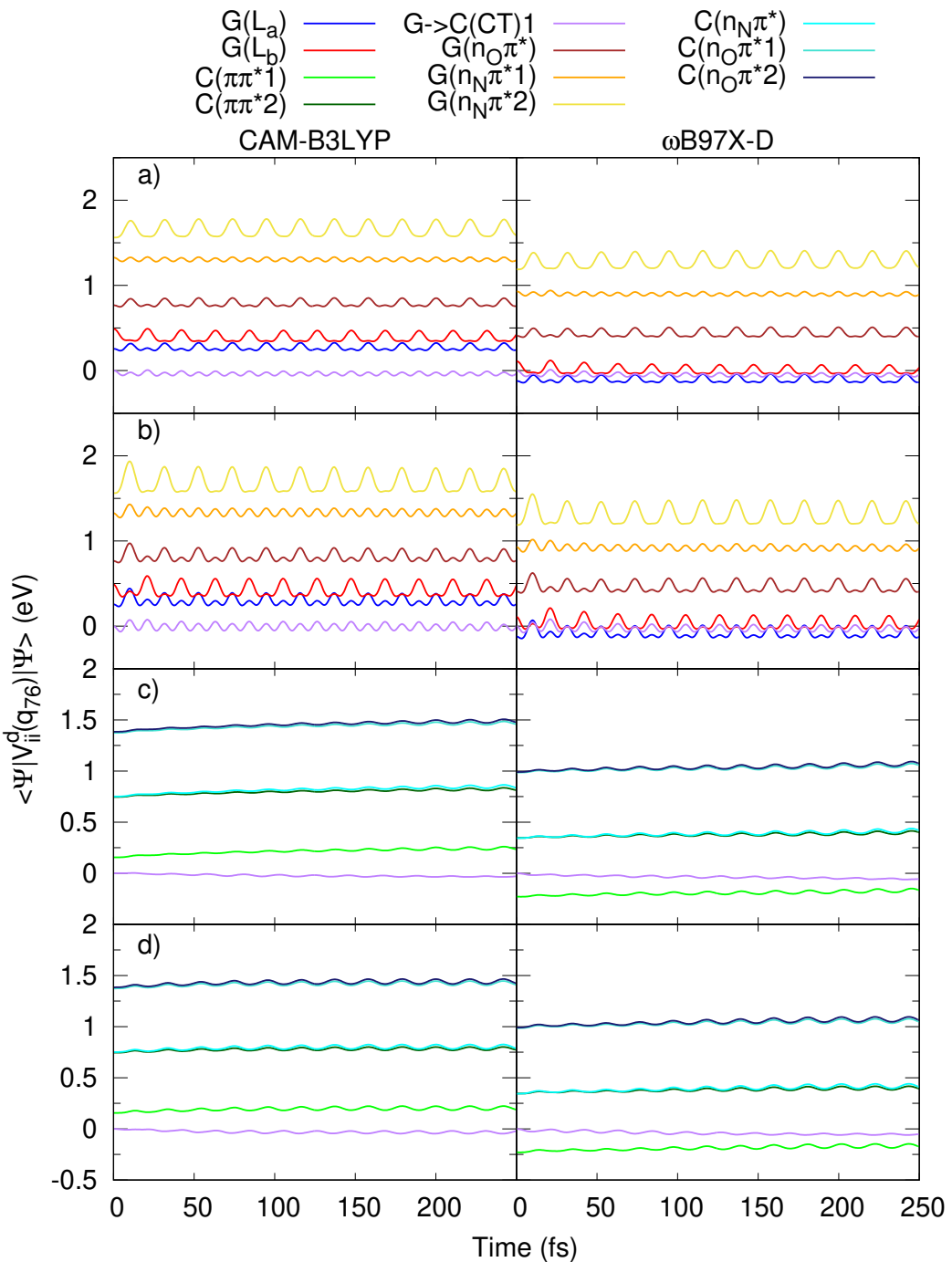


Figure S11: Expectation of diabatic state potential energies along mode  $q_{76}$  ( $\langle \Psi | V_{ii}^d(q_{76}) | \Psi \rangle$ ), shifted by  $-E_{CT1}^d(0) - 1/4\omega_{76}$  that the G $\rightarrow$ C(CT)1 energy is 0 initially. For the 12 state FrD-LVC models for GC, parametrized by left: CAM-B3LYP and right:  $\omega$ B97X-D with 6-31G(d) basis set for dynamics initiated on a) G( $L_a$ ), b) G( $L_b$ ), c) C( $\pi\pi^*1$ ) and d) C( $\pi\pi^*2$ ) states. For clarity, only the potentials of the G $\rightarrow$ C(CT)1 and the  $\pi\pi^*$  and  $n\pi^*$  states localised on the base that is initially excited are shown.

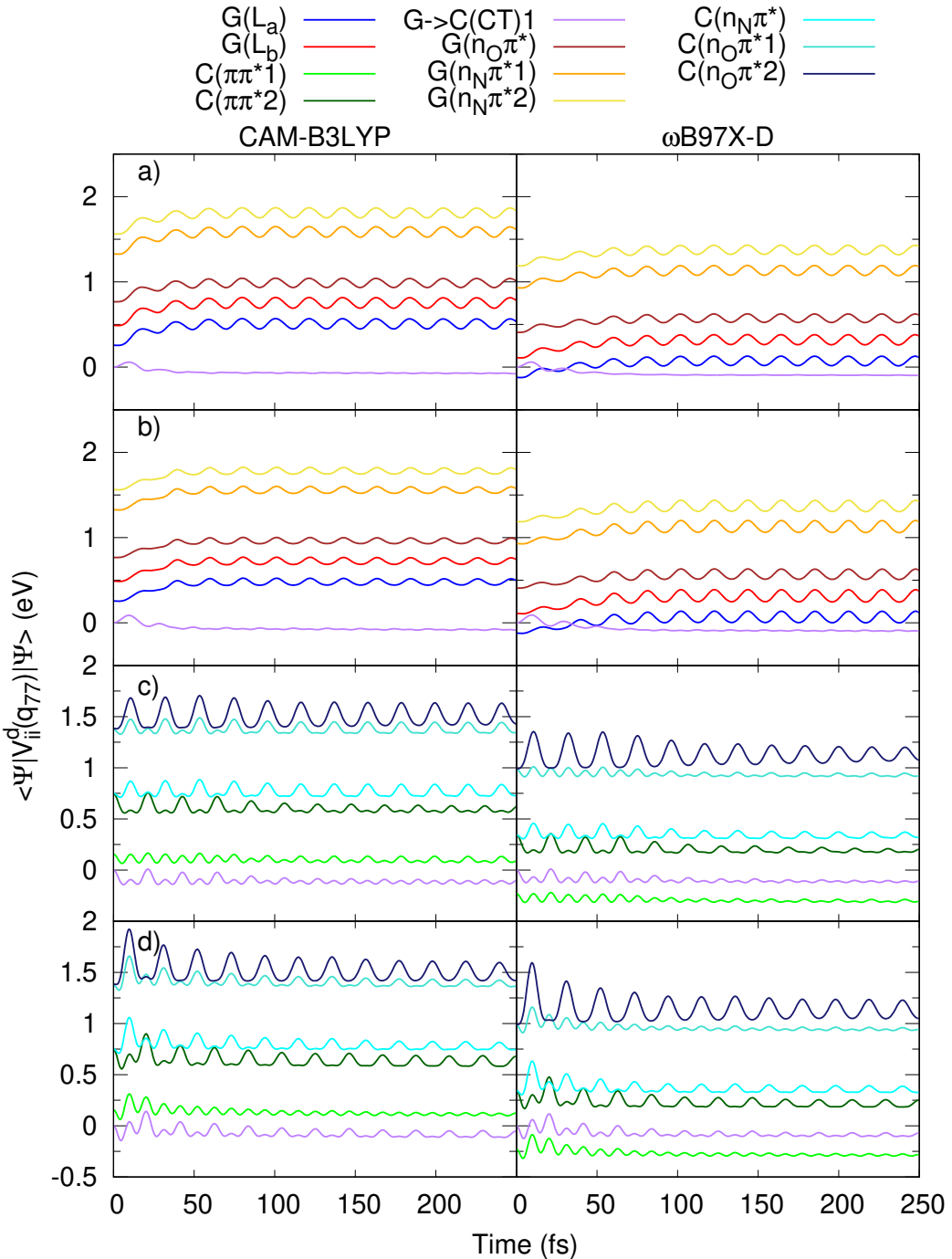


Figure S12: Expectation of diabatic state potential energies along mode  $q_{77}$  ( $\langle \Psi | V_{ii}^d(q_{77}) | \Psi \rangle$ ), shifted by  $-E_{CT1}^d(0) - 1/4\omega_{77}$  so that the  $G \rightarrow C(CT)1$  energy is 0 initially. For the 12 state FrD-LVC models for GC, parametrized by left: CAM-B3LYP and right:  $\omega$ B97X-D with 6-31G(d) basis set for dynamics initiated on a)  $G(L_a)$ , b)  $G(L_b)$ , c)  $C(\pi\pi^*1)$  and d)  $C(\pi\pi^*2)$  states. For clarity, only the potentials of the  $G \rightarrow C(CT)1$  and the  $\pi\pi^*$  and  $n\pi^*$  states localised on the base that is initially excited are shown.

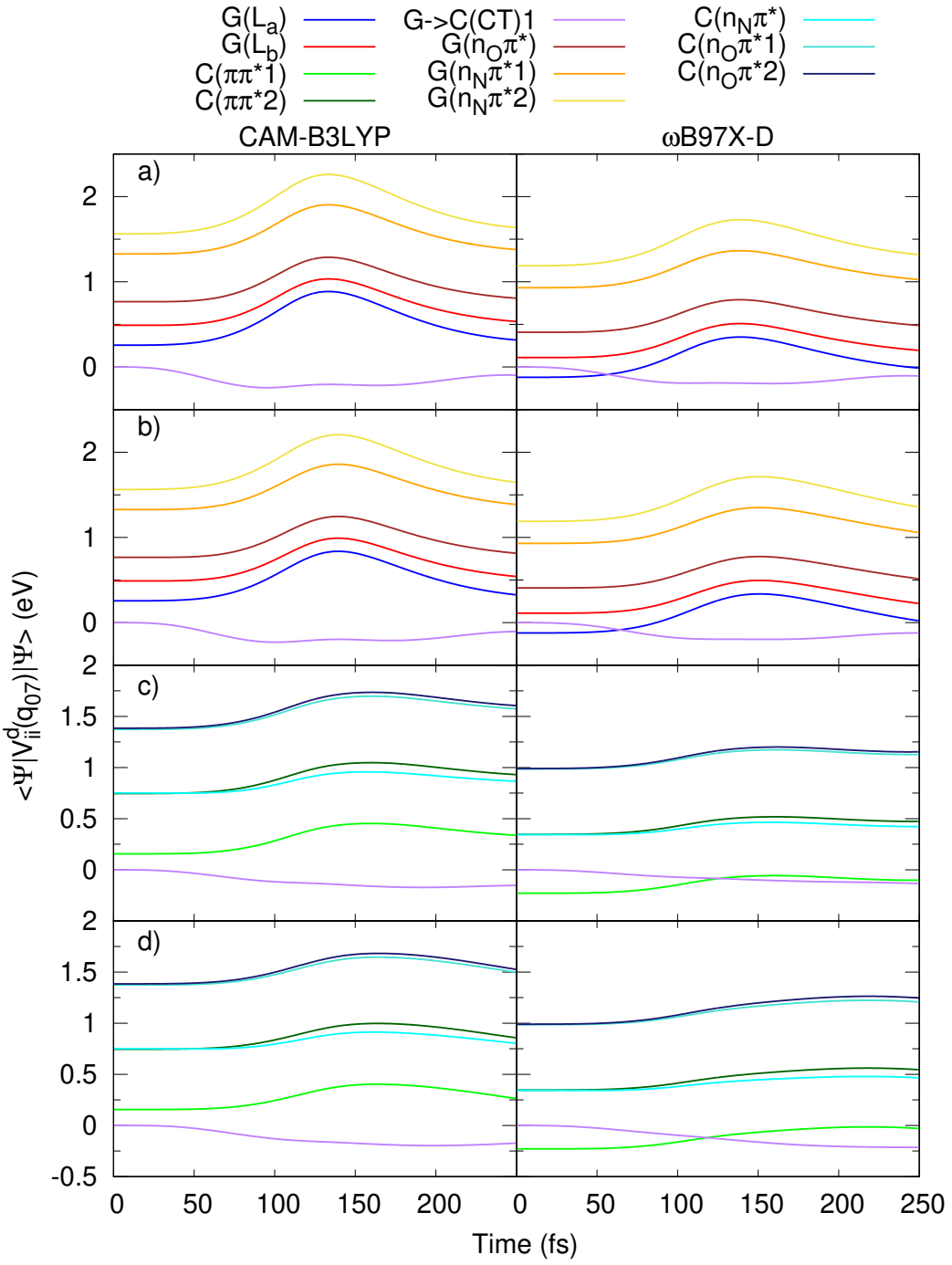


Figure S13: Expectation of diabatic state potential energies along mode  $q_{07}$ , ( $\langle \Psi | V_{ii}^d(q_{07}) | \Psi \rangle$ ) shifted by  $-E_{CT1}^d(0) - 1/4\omega_{07}$  so that the G $\rightarrow$ C(CT)1 energy is 0 initially. For the 12 state FrD-LVC models for GC, parametrized by left: CAM-B3LYP and right:  $\omega$ B97X-D with 6-31G(d) basis set for dynamics initiated on a) G(L<sub>a</sub>), b) G(L<sub>b</sub>), c) C(ππ\*1) and d) C(ππ\*2) states. For clarity, only the potentials of the G $\rightarrow$ C(CT)1 and the ππ\* and nπ\* states localised on the base that is initially excited are shown.

### S4.3 Diabatic Potential Couplings

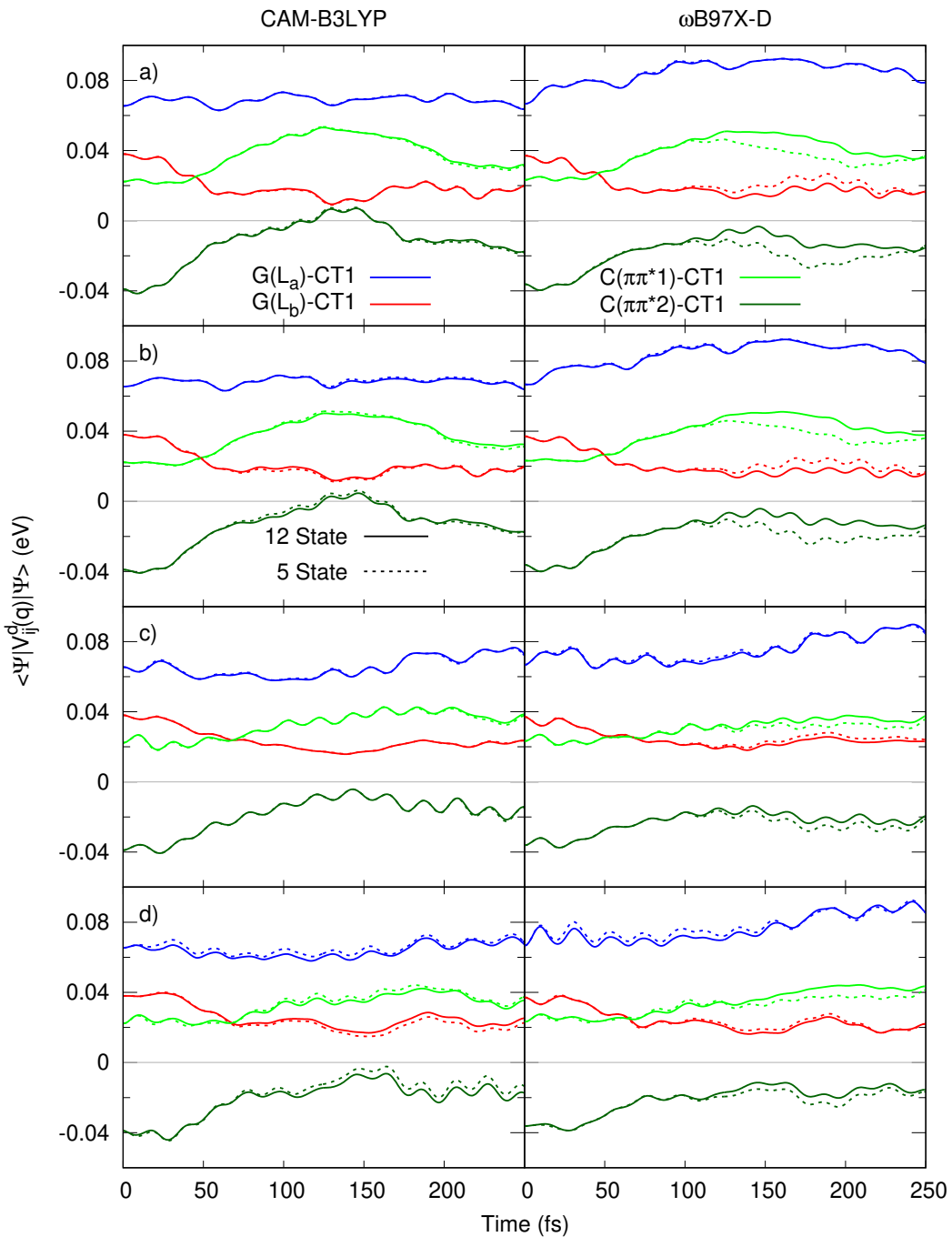


Figure S14: Expectation of  $\pi\pi^*$ -G $\rightarrow$ C(CT)1 diabatic state coupling potential energy, ( $\langle \Psi | V_{ij}^d(q) | \Psi \rangle$ ) for the 12 state (solid lines) and 5 state (dotted lines) FrD-LVC models for GC. Parametrized by left: CAM-B3LYP and right:  $\omega$ B97X-D with 6-31G(d) basis set for dynamics initiated on a)  $G(L_a)$ , b)  $G(L_b)$ , c)  $C(\pi\pi^*1)$  and d)  $C(\pi\pi^*2)$  states.

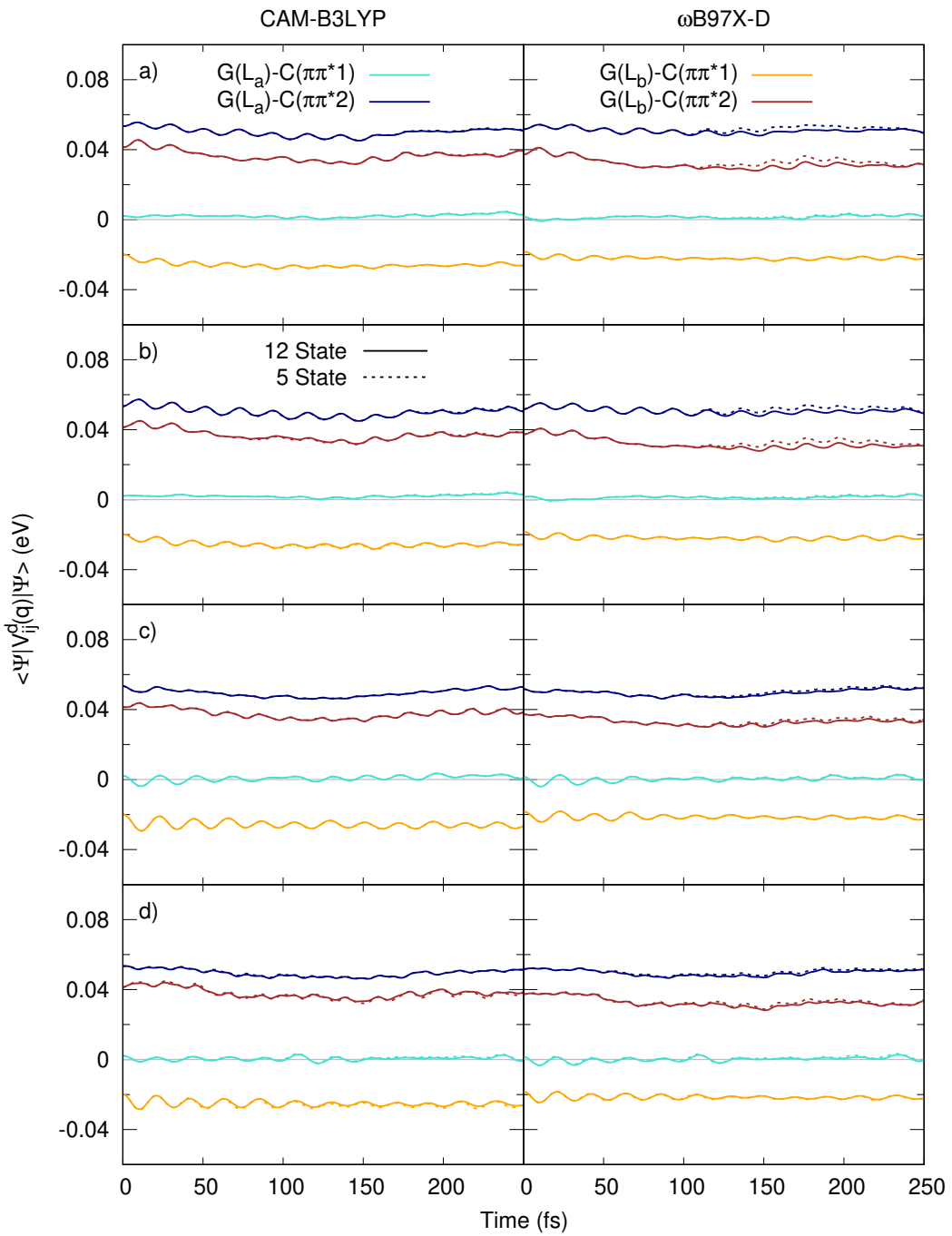


Figure S15: Expectation of excitonic diabatic state coupling potential energy ( $\langle \Psi | V_{ij}^d(q) | \Psi \rangle$ ) for the 12 state (solid lines) and 5 state (dotted lines) FrD-LVC models for GC. Parametrized by left: CAM-B3LYP and right:  $\omega$ B97X-D with 6-31G(d) basis set for dynamics initiated on a) G(L<sub>a</sub>), b) G(L<sub>b</sub>), c) C( $\pi\pi^*1$ ) and d) C( $\pi\pi^*2$ ) states.

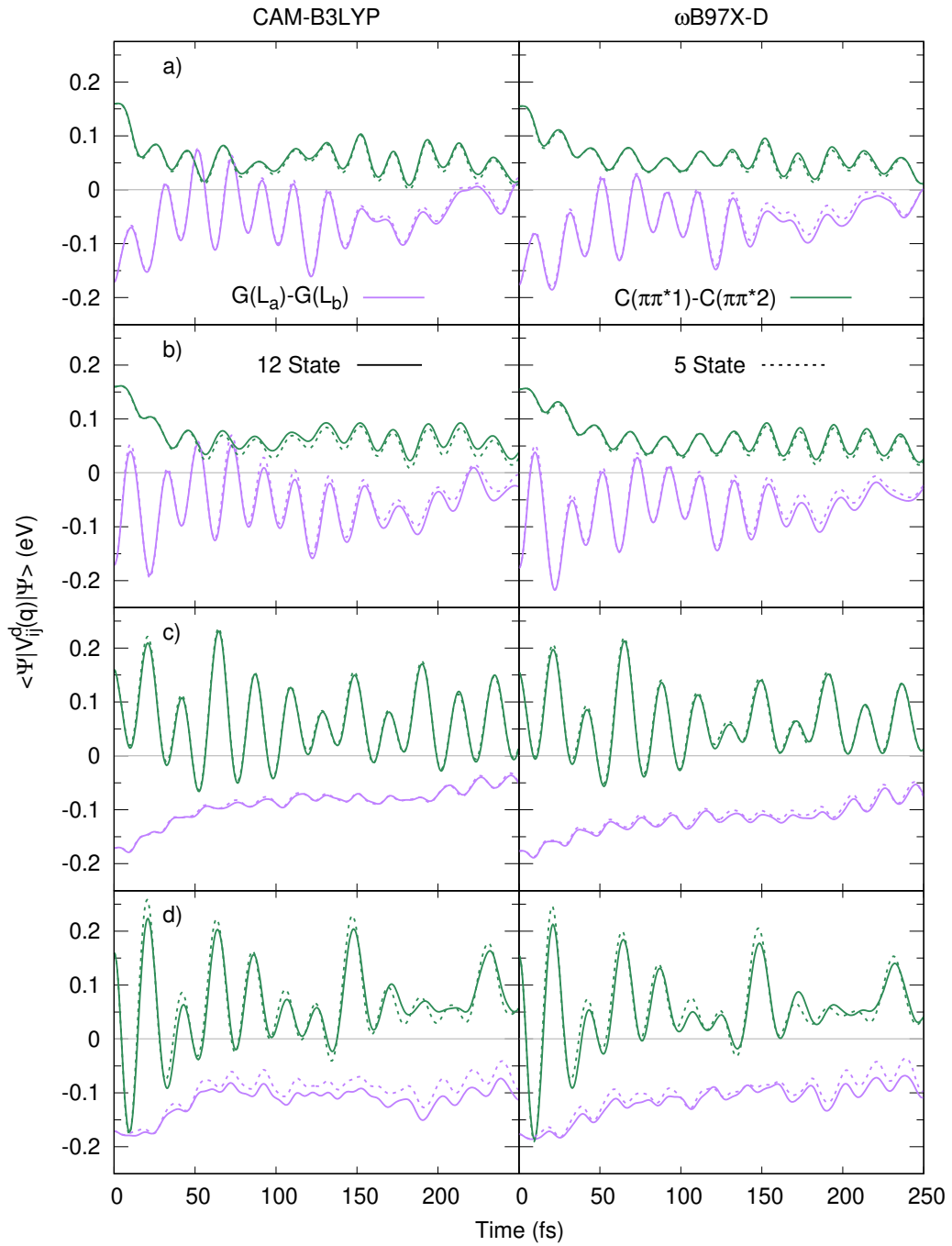


Figure S16: Expectation of the  $\pi\pi^*$  mixing diabatic state coupling potential energy ( $\langle \Psi | V_{ij}^d(q) | \Psi \rangle$ ) for the 12 state (solid lines) and 5 state (dotted lines) FrD-LVC models for GC. Parametrized by left: CAM-B3LYP and right:  $\omega$ B97X-D with 6-31G(d) basis set for dynamics initiated on a)  $G(L_a)$ , b)  $G(L_b)$ , c)  $C(\pi\pi^*1)$  and d)  $C(\pi\pi^*2)$  states.

#### S4.4 Electronic Only Dynamics

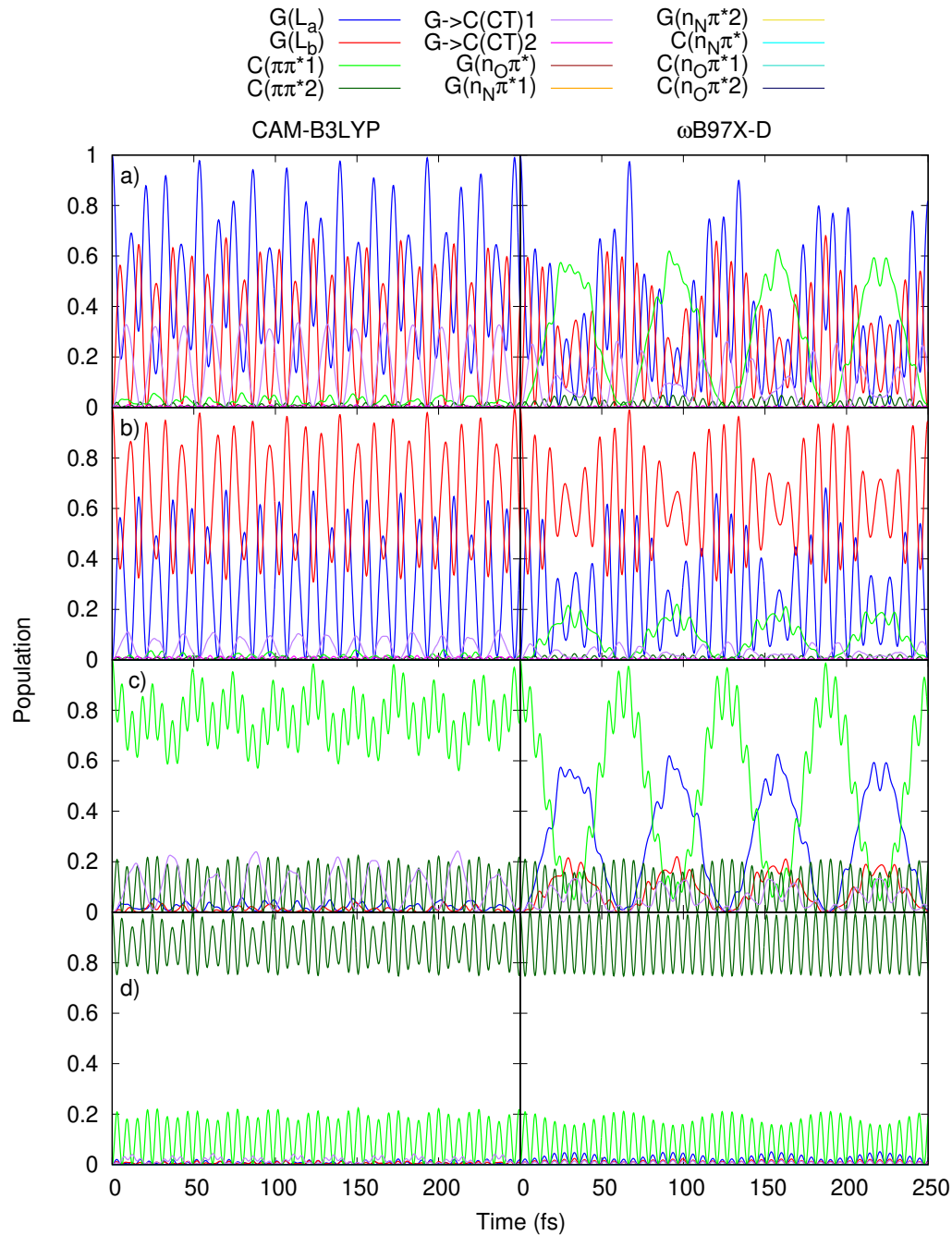


Figure S17: Diabatic state populations for 12 state electronic only dynamics at the FC point. Initiated on a)  $G(L_a)$ , b)  $G(L_b)$ , c)  $C(\pi\pi^*1)$  and d)  $C(\pi\pi^*2)$  states. Parametrized by CAM-B3LYP (left) and  $\omega$ B97X-D (right) with 6-31G(d) basis set.

## S4.5 G $\rightarrow$ C(CT)1 Diabatic Energy Gap Dependence

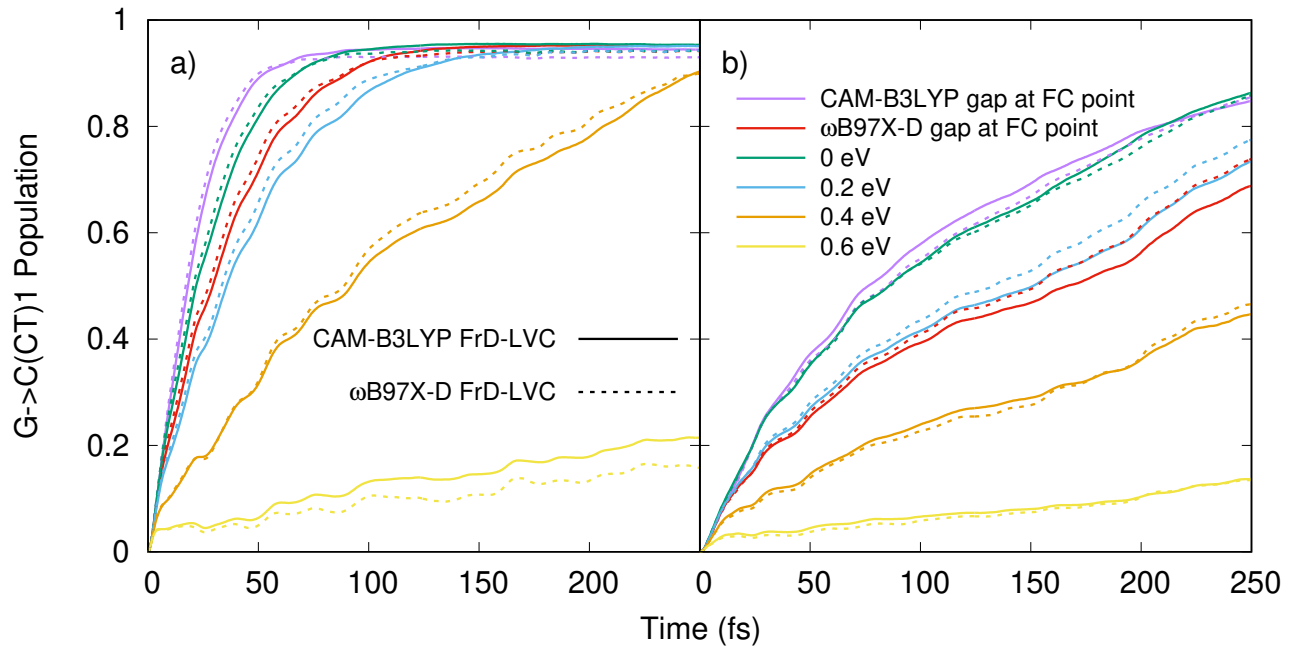


Figure S18: G $\rightarrow$ C(CT)1 populations for 5 state FrD-LVC models parametrized by CAM-B3LYP (solid lines) and  $\omega$ B97X-D (dashed lines) with 6-31G(d) basis set, with different diabatic energy gaps between the  $\pi\pi^*$  state of initial excitation and G $\rightarrow$ C(CT)1 state (i.e.  $E_{\text{CT}1}^{\text{d}}(0) - E_{\pi\pi^*}^{\text{d}}(0)$ ) for dynamics initiated on a) G(L<sub>a</sub>) and b) C( $\pi\pi^*$ 1). The purple line is the CAM-B3LYP gap obtained by FrD at the FC point (-0.26 eV for G $\rightarrow$ C(CT)1-G(L<sub>a</sub>) and -0.16 eV for G $\rightarrow$ C(CT)1-C( $\pi\pi^*$ 1)), the red line is the  $\omega$ B97X-D gap obtained by FrD at the FC point (0.12 eV for G $\rightarrow$ C(CT)1-G(L<sub>a</sub>) and 0.23 eV for G $\rightarrow$ C(CT)1-C( $\pi\pi^*$ 1)).

## S5 Additional Absorption Spectra

### S5.1 Comparison To Experimental Absorption Spectrum in Chloroform

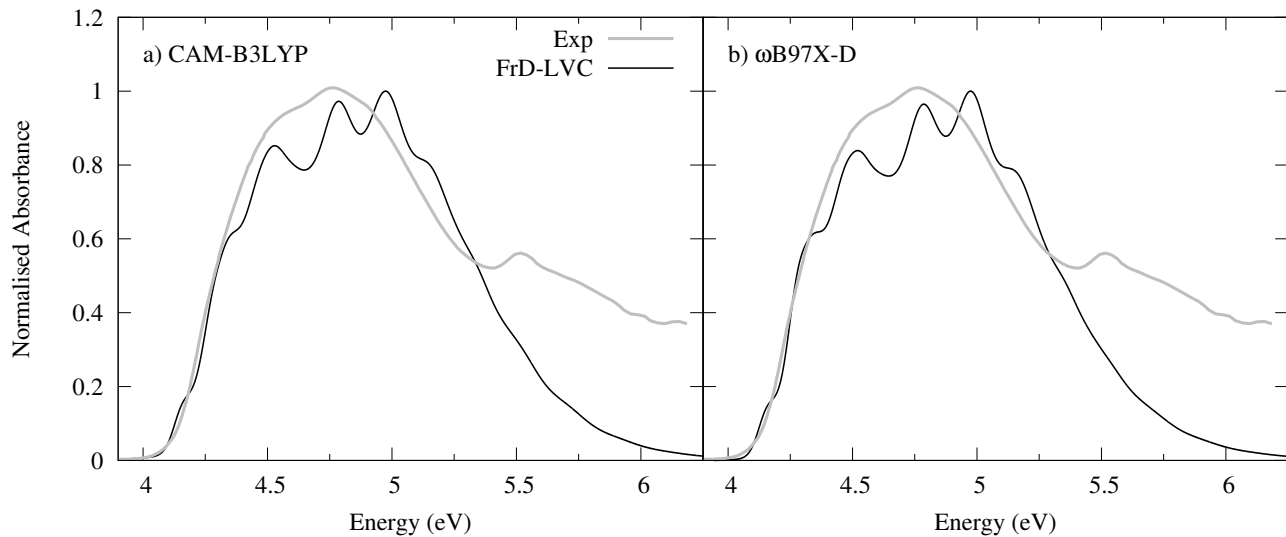


Figure S19: Absorption spectra of GC calculated from the 12 state FrD-LVC models (solid black lines) parametrized by a) CAM-B3LYP and b)  $\omega$ B97X-D with 6-31G(d) basis set, compared to experimental results in chloroform.<sup>9</sup> Intensity of most intense peaks normalised to 1, plotted on the energy scale, with FrD-LVC spectra shifted by -0.75 eV.

## S6 6-31+G(d,p) Basis Set Test

### S6.1 Single Point Energies

Table S16: TD-DFT excitation energies (eV) of GC in  $C_s$  symmetry at equilibrium geometry obtained with the CAM-B3LYP and  $\omega$ B97X-D functionals and 6-31G(d) and 6-31+G(d,p) basis sets. Also shown are EOM-CCSD(T)/TZVP results from Ref. 10.

Char.	CAM-B3LYP		$\omega$ B97X-D		EOM-CCSD(T)
	6-31+G(d,p)	6-31G(d)	6-31+G(d,p)	6-31G(d)	
G→C(CT)1	4.89 (S <sub>1</sub> )	5.07 (S <sub>1</sub> )	5.46 (S <sub>4</sub> )	5.50 (S <sub>3</sub> )	5.36
C( $\pi\pi^*$ )	5.15 (S <sub>2</sub> )	5.27 (S <sub>2</sub> )	5.15 (S <sub>2</sub> )	5.28 (S <sub>2</sub> )	4.92
G(L <sub>a</sub> )	5.21 (S <sub>3</sub> )	5.31 (S <sub>3</sub> )	5.01 (S <sub>1</sub> )	5.21 (S <sub>1</sub> )	4.85
G(L <sub>b</sub> )	5.39 (S <sub>5</sub> )	5.69 (S <sub>4</sub> )	5.44 (S <sub>3</sub> )	5.69 (S <sub>4</sub> )	5.48
C(n <sub>N</sub> $\pi^*$ )	5.71 (S <sub>6</sub> )	5.79 (S <sub>5</sub> )	5.71 (S <sub>6</sub> )	5.77 (S <sub>5</sub> )	5.65
G(n <sub>O</sub> $\pi^*$ )	5.86 (S <sub>9</sub> )	5.93 (S <sub>6</sub> )	5.86 (S <sub>8</sub> )	5.93 (S <sub>7</sub> )	5.76
C( $\pi\pi^*$ 2)	5.73 (S <sub>7</sub> )	5.93 (S <sub>7</sub> )	5.73 (S <sub>7</sub> )	5.90 (S <sub>6</sub> )	5.37
G→C(CT)2	6.14 (S <sub>13</sub> )	6.33 (S <sub>8</sub> )	6.54 (S <sub>17</sub> )	6.60 (S <sub>11</sub> )	
G(n <sub>N</sub> $\pi^*$ 1)	6.30 (S <sub>14</sub> )	6.44 (S <sub>9</sub> )	6.30 (S <sub>10</sub> )	6.43 (S <sub>8</sub> )	
C(n <sub>O</sub> $\pi^*$ 1)	6.40 (S <sub>17</sub> )	6.45 (S <sub>10</sub> )	6.42 (S <sub>14</sub> )	6.46 (S <sub>9</sub> )	6.27
C(n <sub>O</sub> $\pi^*$ 2)	6.51 (S <sub>20</sub> )	6.60 (S <sub>11</sub> )	6.48 (S <sub>16</sub> )	6.56 (S <sub>10</sub> )	6.42
G(n <sub>N</sub> $\pi^*$ 2)	6.56 (S <sub>21</sub> )	6.71 (S <sub>12</sub> )	6.56 (S <sub>18</sub> )	6.70 (S <sub>12</sub> )	

Table S16 shows the vertical excitation energies calculated by the CAM-B3LYP and  $\omega$ B97X-D functionals with the 6-31+G(d,p) basis set, compared to the results of the 6-31G(d) basis set shown in the main text, and the EOM-CCSD(T)/TZVP results from Ref. 10. TD-DFT excitation energies calculated following geometry optimisation of GC with the same functional and basis set. The calculations with 6-31+G(d,p) yielded a large number of Rydberg states, not shown in the Table, and a slight red-shifting of the  $\pi\pi^*$ , n $\pi^*$  and CT energies. For both functionals, there is a  $\sim$ 0.1 eV red-shift of the n $\pi^*$  states, and a  $\sim$ 0.1-0.3 red-shift of the  $\pi\pi^*$  states, whilst the CT states are predicted to be  $\sim$ 0.2 eV red-shifted by CAM-B3LYP and  $\sim$ 0.05 eV red-shifted by  $\omega$ B97X-D. The relative ordering of the states, however, is quite similar between the basis sets.

## S6.2 $\omega$ B97X-D 6-31+G(d,p) FrD-LVC Model

Table S17: Diabatic energies ( $E_{ii}^d(0)$ ) and electronic couplings ( $E_{ij}^d(0)$ ) of  $n\pi^*$  states of GC in  $C_s$  symmetry at equilibrium geometry from a 12 state FrD-LVC model parametrized by  $\omega$ B97X-D/6-31+G(d,p) (eV).

	$G \rightarrow C(CT)1$	$C(\pi\pi^*1)$	$G(L_a)$	$G(L_b)$	$C(\pi\pi^*2)$	$G \rightarrow C(CT)2$
$G \rightarrow C(CT)1$	5.417					
$C(\pi\pi^*1)$	0.037	5.198				
$G(L_a)$	0.133	-0.003	5.227			
$G(L_b)$	0.058	-0.020	-0.156	5.409		
$C(\pi\pi^*2)$	-0.048	0.161	0.062	0.041	5.709	
$G \rightarrow C(CT)2$	-0.097	-0.002	-0.036	0.052	-0.008	6.487

Table S18: Diabatic energies ( $E_{ii}^d(0)$ ) and electronic couplings ( $E_{ij}^d(0)$ ) of  $n\pi^*$  states of GC in  $C_s$  symmetry at equilibrium geometry from a 12 state FrD-LVC model parametrized by  $\omega$ B97X-D/6-31+G(d,p) (eV).

	$C(n_N\pi^*)$	$G(n_O\pi^*)$	$G(n_N\pi^*1)$	$C(n_O\pi^*1)$	$C(n_O\pi^*2)$	$G(n_N\pi^*2)$
$C(n_N\pi^*)$	5.829					
$G(n_O\pi^*)$	-0.012	5.869				
$G(n_N\pi^*1)$	-0.003	-0.058	6.318			
$C(n_O\pi^*1)$	-0.007	-0.004	-0.003	6.484		
$C(n_O\pi^*2)$	-0.010	0.000	0.001	-0.034	6.449	
$G(n_N\pi^*2)$	-0.014	-0.016	-0.067	-0.006	0.004	6.573

We performed a test on the effect of basis set on the dynamics, by parametrizing 12 state and 5 state FrD-LVC models with the 6-31+G(d,p) basis set and  $\omega$ B97X-D functional. The population dynamics after propagation by ML-MCTDH with these models is shown in Figure S20. Similar conclusions to the main text are found, namely: fast and efficient transfer from initially excited  $\pi\pi^*$  state to the  $G \rightarrow C(CT)1$  state that is quicker for an initial excitation on  $G$  than  $C$ ; the  $G(L_a)$  and  $C(\pi\pi^*1)$  states act as doorway states to  $G \rightarrow C(CT)1$ ; there is limited involvement of the  $n\pi^*$  states; a reduced dimensionality (5 state) model can reproduce the population dynamics of the full dimensional (12 state) model; and there is limited dependence of the  $\pi\pi^*$ - $G \rightarrow C(CT)1$  coupling on coordinate. The main difference to the models presented in the main text concerns the rate at which the  $G \rightarrow C(CT)1$  state is populated, with it being faster for this 6-31+G(d,p) basis set parametrized model. The reason for this is due to larger constant coupling terms ( $E_{ij}^d(0)$ ) between the  $\pi\pi^*$  and  $G \rightarrow C(CT)1$  state, as shown in Table S17. This is despite a slightly larger energy gap between the  $G \rightarrow C(CT)1$  and  $\pi\pi^*$  doorway states, as shown in Tables S16 and S17.

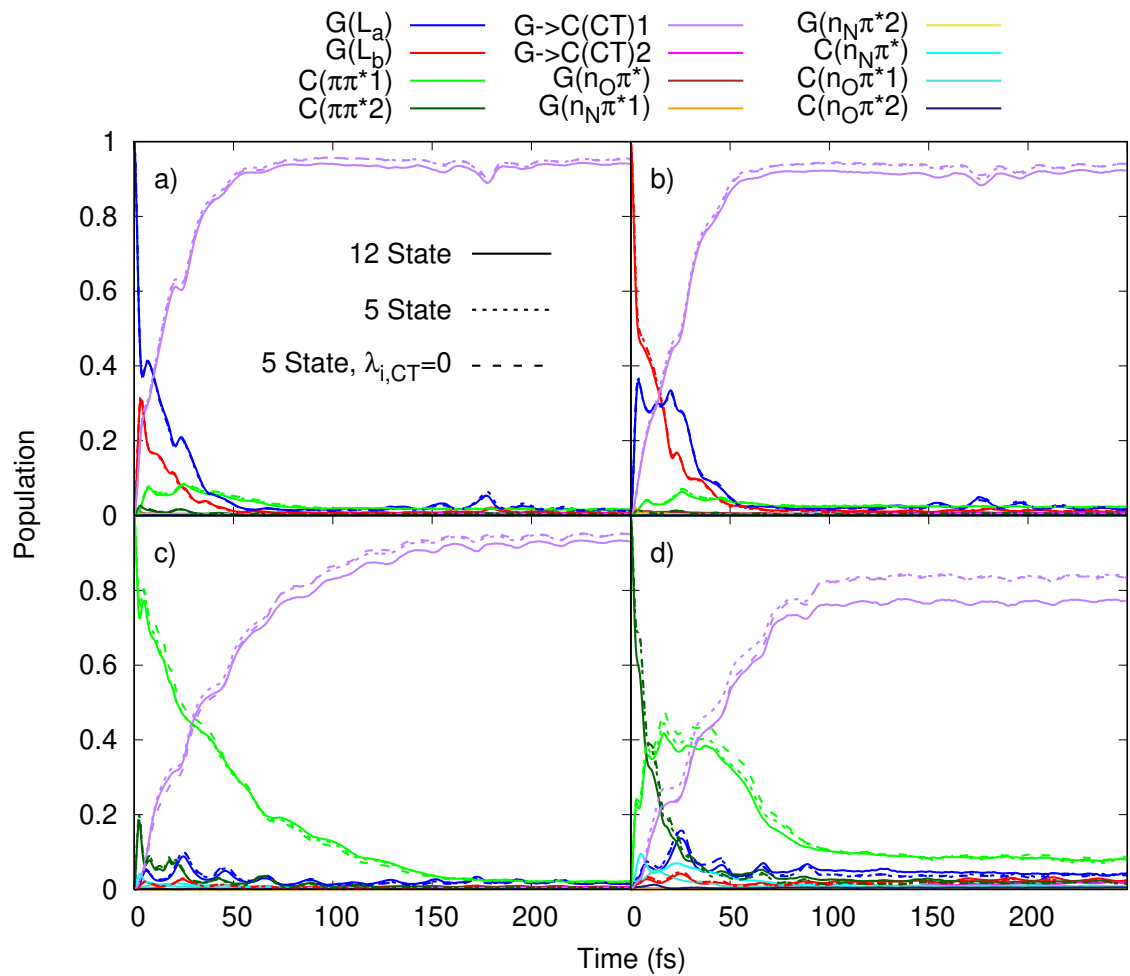


Figure S20: Diabatic state populations for FrD-LVC models with 12 states (solid line), 5 states (dotted line), and 5 states with  $\lambda_{ij} = 0$  for all the  $\pi\pi^*$  states coupled to CT (dashed line). Dynamics initiated on a)  $G(L_a)$ , b)  $G(L_b)$ , c)  $C(\pi\pi^*1)$  and d)  $C(\pi\pi^*2)$  states. Parametrized by  $\omega B97X-D/6-31+G(d,p)$ .

## References

- [1] Johannes Neugebauer, Evert Jan Baerends, and Marcel Nooijen, "Vibronic coupling and double excitations in linear response time-dependent density functional calculations: Dipole-allowed states of n<sub>2</sub>", *J. Chem. Phys.* **121**(13), pp. 6155–6166 (2004).
- [2] Yanli Liu, Javier Cerezo, Na Lin, Xian Zhao, Roberto Improta, and Fabrizio Santoro, "Comparison of the results of a mean-field mixed quantum/classical method with full quantum predictions for nonadiabatic dynamics: application to the  $\pi\pi^*/n\pi^*$  decay of thymine", *Theor. Chem. Acc.* **137**, pp. 40 (2018).
- [3] Yanli Liu, Lara Martínez Fernández, Javier Cerezo, Giacomo Prampolini, Roberto Improta, and Fabrizio Santoro, "Multistate coupled quantum dynamics of photoexcited cytosine in gas-phase: Nonadiabatic absorption spectrum and ultrafast internal conversions.", *Chem. Phys.* **515**, pp. 452–463 (2018).
- [4] Martha Yaghoubi Jouybari, Yanli Liu, Roberto Improta, and Fabrizio Santoro, "Ultrafast dynamics of the two lowest bright excited states of cytosine and 1-methylcytosine: A quantum dynamical study", *J. Chem. Theory Comput.* **16**(9), pp. 5792–5808 (2020).
- [5] Martha Yaghoubi Jouybari, Yanli Liu, Roberto Improta, and Fabrizio Santoro, "Quantum dynamics of the  $\pi\pi^*/n\pi^*$  decay of the epigenetic nucleobase 1,5-dimethyl-cytosine in the gas phase", *Phys. Chem. Chem. Phys.* **22**, pp. 26525–26535 (2020).
- [6] James A. Green, Martha Yaghoubi Jouybari, Daniel Aranda, Roberto Improta, and Fabrizio Santoro, "Nonadiabatic absorption spectra and ultrafast dynamics of dna and rna photoexcited nucleobases", *Molecules* **26**(6) (2021).
- [7] James A. Green, Haritha Asha, Fabrizio Santoro, and Roberto Improta, "Excitonic model for strongly coupled multichromophoric systems: The electronic circular dichroism spectra of guanine quadruplexes as test cases", *J. Chem. Theory Comput.* **17**(1), pp. 405–415 (2021).
- [8] Kinga E. Szkaradek, Petr Stadlbauer, Jiří Šponer, Robert W. Góra, and Rafał Szabla, "Uv-induced hydrogen transfer in dna base pairs promoted by dark  $n\pi^*$  states", *Chem. Commun.* **56**, pp. 201–204 (2020).
- [9] N. K. Schwalb and F. Temps, "Ultrafast electronic relaxation in guanosine is promoted by hydrogen bonding with cytidine", *J. Am. Chem. Soc.* **129**, pp. 9272 (2007).
- [10] Péter G. Szalay, Thomas Watson, Ajith Perera, Victor Lotrich, and Rodney J. Bartlett, "Benchmark studies on the building blocks of dna. 3. watson–crick and stacked base pairs", *J. Phys. Chem. A* **117**(15), pp. 3149–3157 (2013).